NEURAL JUMP ORDINARY DIFFERENTIAL EQUATIONS

Anonymous authors
Paper under double-blind review

ABSTRACT

Combinations of neural ODEs with recurrent neural networks (RNN), like GRU-ODE-Bayes or ODE-RNN are well suited to model irregularly observed time series. While those models outperform existing discrete-time approaches, no theoretical guarantees for their predictive capabilities are available. Assuming that the irregularly-sampled time series data originates from a continuous stochastic process, the L^2-optimal online prediction is the conditional expectation given the currently available information. We introduce the neural jump ODE (NJ-ODE) that provides a data-driven approach to learn, continuously in time, the conditional expectation of a stochastic process. Our approach models the conditional expectation between two observations with a neural ODE and jumps whenever a new observation is made. We define a novel training framework, which allows us to prove theoretical guarantees for the first time. In particular, we show that the output of our model converges to the L^2-optimal prediction. We provide experiments showing that the theoretical results also hold empirically. Moreover, we experimentally show that our model outperforms the baselines in more complex learning tasks and give comparisons on real-world datasets.

1 INTRODUCTION

Stochastic processes are widely used in many fields to model time series that exhibit a random behaviour. In this work, we focus on processes that can be expressed as solutions of stochastic differential equations (SDE) of the form

$$dX_t = \mu(t, X_t)dt + \sigma(t, X_t)dW_t \,,$$

with certain assumptions on the drift μ and the diffusion σ. With respect to the L^2-norm, the best prediction of a future value of the process is provided by the conditional expectation given the current value. If the drift and diffusion are known or a good estimation is available, the conditional expectation can be approximated by a Monte Carlo (MC) simulation. However, since μ and σ are usually unknown, this approach strongly depends on the assumptions made on their parametric form. A more flexible approach is given by *neural SDEs*, where the drift μ and diffusion σ are modelled by neural networks (Tzen & Raginsky, 2019; Li et al., 2020; Jia & Benson, 2019). Nevertheless, modelling the diffusion can be avoided if one is only interested in forecasting the behaviour instead of sampling new paths.

An alternative widely used approach is to use Recurrent Neural Networks (RNN), where a neural network dynamically updates a latent variable with the observations of a discrete input time-series. RNNs are successfully applied to tasks for which time-series are regularly sampled, as for example speech or text recognition. However, often observations are irregularly observed in time. The standard approach of dividing the time-line into equally-sized intervals and imputing or aggregating observations might lead to a significant loss of information (Rubanova et al., 2019). Frameworks that overcome this issue are the GRU-ODE-Bayes (Brouwer et al., 2019) and the ODE-RNN (Rubanova et al., 2019), which combine a RNN with a *neural ODE* (Chen et al., 2018). In standard RNNs, the hidden state is updated at each observation and constant in between. Conversely, in the GRU-ODE-Bayes and ODE-RNN framework, a neural ODE is trained to model the continuous evolution of the hidden state of the RNN between two observations. While GRU-ODE-Bayes and ODE-RNN both provide convincing empirical results, they lack thorough theoretical guarantees.

Contribution. In this paper, we introduce a mathematical framework to precisely describe the problem statement of online prediction of a stochastic process with temporal irregular observations.

Based on this rigorous mathematical description, we introduce the Neural Jump ODE (NJ-ODE). The model architecture is very similar to the one of GRU-ODE-Bayes and ODE-RNN, however we introduce a novel training framework, which in contrast to them allows us to prove convergence guarantees for the first time. Moreover, we demonstrate empirically the capabilities of our model.

Precise problem formulation. We emphasize that a precise definition of all ingredients is needed, to be able to show theoretical convergence guarantees, which is the main purpose of this work. Since the objects of interest are stochastic processes, we use tools from probability theory and stochastic calculus. To make the paper more readable and comprehensible also for people without background in probability theory and stochastic calculus, the precise formulations and demonstrations of all claims are given in the appendix, while the main part of the paper focuses on giving well understandable heuristics.

2 PROBLEM STATEMENT

The problem we consider in this work, is the online forecasting of temporal data. In particular, we assume that we make observations of a stochastic process described by the stochastic differential equation (SDE)

$$dX_t = \mu(t, X_t)dt + \sigma(t, X_t)dW_t \,, \tag{1}$$

at irregularly-sampled time points. Between those observation times, we want to predict the stochastic process, based only on the observations that we made previously in time, excluding the possibility to interpolate observations. In other words, online forecasting means, that after each observation we want to extrapolate the current and the previous observations into the future until we make the next observation. The time at which the next observation will be made is random and assumed to be independent of the stochastic process itself.

More precisely, we suppose to observe N realisations of the $\mathbb{R}^{d_X}$-dimensional stochastic process X defined in (1). Each realisation j is observed at n_j random observation times $t_1^j, \dots, t_{n_j}^j \in [0, T]$ with values $x_1^j, \dots, x_{n_j}^j \in \mathbb{R}^{d_X}$. We assume that all coordinates of x_i^j are observed.

We are interested in forecasting how a new realization evolves in time, such that our predictions minimize the expected squared distance (L^2-metric) to the true unknown value. The optimal prediction, i.e. the L^2-minimizer, is the conditional expectation. Given that the value of the realization at time t is x_t, we are therefore interested in estimating the function

$$f_{(x_t,t)}(s) := E[X_{t+s}|X_t = x_t], \; s > 0. \tag{2}$$

To estimate $f_{(x,t)}(s)$ we make use of the N realizations that were observed before. The following example illustrates the considered problem.

Example. Several blood values and hormone values of participants in a health study are measured at body checks multiple times during one year. Each participant has his checks depending on the schedule of the study and his own schedule, hence the observation dates are irregular in time and exhibit some randomness which is independent of the measured values. During the year, participant 1 has his $n_1 = 4$ checks at days $(t_1^1, t_2^1, t_3^1, t_4^1) = (7, 142, 227, 355)$ where the values $(x_1^1, x_2^1, x_3^1, x_4^1) = (0.74, 0.65, 0.78, 0.81)$ are measured. Participant 2 only has $n_2 = 2$ checks at days $(t_1^2, t_2^2) = (89, 257)$ where the values $(x_1^2, x_2^2) = (0.56, 0.63)$ are measured. Similarly, the j-th patient has his n_j checks at the dates $(t_1^j, \dots, t_{n_j}^j)$ and has the measured values $(x_1^j, \dots, x_{n_j}^j)$. Based on this data, we want to forecast the blood and hormone values of patients in hospitals. In particular, for a patient with measured values x_1 at time t_1, we want to predict what his values will likely be at any time $t_1 + s > t_1$. Importantly, we do not only focus on predicting the values at some $t_2 > t_1$, but we want to know the entire evolution of the values.

3 BACKGROUND

Recurrent Neural Network. The input to a RNN is a discrete time series of observations $\{x_{t_1}, \cdots, x_{t_n}\}$. At each time t_{i+1}, the latent variable h is updated using the previous latent variable h_i and the input x_{i+1} as

$$h_{i+1} := \text{RNNCell}(h_i, x_{i+1}), \tag{3}$$

where RNNCell is a neural network.

Neural Ordinary Differential Equation. Neural ODEs (Chen et al., 2018) are a family of continuous-time models defining a latent variable $h_t := h(t)$ to be the solution to an ODE initial-value problem (IVP):

$$h_i := h_0 + \int_{t_0}^{t_i} f(h_s, s, \theta) ds, \quad t \geq t_0, \tag{4}$$

where $f(\cdot, \cdot, \theta) = f_\theta$ is a neural network with weights θ. Therefore, the latent variables can be updated continuously by solving this ODE (4). We can emphasize the dependence of h_t on a numerical ODE solver by rewriting (4) as

$$h_i := \text{ODESolve}(f_\theta, h_0, (t_0, t_i)) \,. \tag{5}$$

ODE-RNN. ODE-RNN (Rubanova et al., 2019) is a mixture of a RNN and a neural ODE. In contrast to a standard RNN, we are not only interested in an output at the observation times t_i, but also in between those times. In particular, we want to have an output stream that is generated continuously in time. This is achieved by using a neural ODE to model the latent dynamics between two observation times, i.e. for $t_i < t < t_{i+1}$ the latent variable is defined as in (4) and (5), with h_{t_0} and t_0 replaced by h_{t_i} and t_i. At the next observation time t_{i+1}, the latent variable is then updated by a RNN. Rubanova et al. (2019) write this as

$$\begin{cases} h'_i & := & \text{ODESolve}(f_\theta, h_{i-1}, (t_{i-1}, t_i)) \\ h_i & := & \text{RNNCell}(h'_{i-1}, x_{i-1}) \,. \end{cases} \tag{6}$$

Therefore, fixing $h_{t_0} := h_0$, the entire latent process can be computed by iteratively solving an ODE followed by applying a RNN.

GRU-ODE-Bayes. The model architecture describing the latent variable in GRU-ODE-Bayes (Brouwer et al., 2019) is defined as a special case of the ODE-RNN architecture. In particular, a gated recurrent unit (GRU) is used for the RNN-cell and a continuous version of the GRU for the neural ODE f_θ. Therefore, we focus on explaining the difference between our model architecture and the ODE-RNN architecture, in the following section.

4 Proposed method – Neural Jump ODE

Markovian paths. Our assumptions on the stochastic process X imply that it is a Markov process. In particular, the optimal prediction of a future state of X only depends on the current state rather than on the full history. Hence, the previous values do not provide any additional useful information for the prediction.

JumpNN instead of RNN. Using a neural ODE between two observation has the advantage that it allows to continuously model the hidden state between two observations. But since the underlying process is Markov, there is no need to use a RNN-cell to model the updates of the hidden state at each new observation. Instead, whenever a new observation is made, the new hidden state can solely be defined from this observation. Therefore, we replace the RNN-cell used in ODE-RNN by a standard neural network mapping the observation to the hidden state. We call this the JumpNN which can be interpreted as an encoder map. The advantage over the ODE-RNN is that this architecture is easier to train.

Last observation and time increment as additional inputs for the neural ODE. The neural network f_θ used in the neural ODE takes two arguments as inputs, the hidden state h_t and the current time t. However, our theoretical problem analysis suggests, that instead of t the last observation time t_{i-1} and the time increment $t - t_{i-1}$ should be used. Additionally the last observation x_{i-1} should also be part of the input. Therefore, we change the input to f_θ accordingly.

Use of hyperbolic tangent. The observations x_i and the hidden states h_t are a priori not bounded. However, it is well known that neural networks work best, if their inputs are bounded by 1. Moreover, bounded inputs are essential in our theoretical analysis to be able to apply universal approximation theorems. Therefore, we apply the $\tanh$ function to all possibly unbounded inputs of the neural networks before passing them on. For better readability, we use the same notation for the inputs x_i and h_t to which $\tanh$ was applied.

NJ-ODE. Combine the ODE-RNN model architecture with the previous considerations, we introduce the modified model architecture of our neural jump ODE (NJ-ODE) model, that can be written similar to (22) as

$$\begin{cases} h'_{i+1} & := & \text{ODESolve}(f_\theta, (h_t, x_i, t_i, t - t_i), (t_i, t_{i+1})) \\ h_{i+1} & := & \text{JumpNN}(x_{i+1}) \,. \end{cases} \tag{7}$$

An implementable version of this method is presented in the Algorithm 1. A neural ODE f_θ transforms the hidden state between observations, and the hidden state jumps according to JumpNN when a new observation is available. The outputNN, a standard neural network, maps any hidden state h_t to the output y_t. To implement the continuous-in-time ODE evaluation, a discretization scheme is provided by the inner loop. In the training process, the weights of all three neural networks, JumpNN, the neural ODE f_θ and outputNN are optimized.

Algorithm 1 The NJ-ODE. A small step size Δt is fixed and we denote $t_{n+1} := T$.

```
Input: Data points with timestamps {(x_i, t_i)}_{i=0...n},
for i = 0 to n do
    h_{t_i} = JumpNN(x_i)                                  ▷ Update hidden state given next observation x_i
    y_{t_i} = outputNN(h_{t_i})                            ▷ compute output
    s ← t_i
    while s + Δt ≤ t_{i+1} do
        h_{s+Δt} = ODESolve(f_θ, h_s, x_i, t_i, s − t_i, (s, s + Δt))   ▷ get next hidden state
        y_{s+Δt} = outputNN(h_{s+Δt})                      ▷ compute output
        s ← s + Δt
    end while
end for
```

Objective function. As described before, our goal is to train the NJ-ODE model such that its output approximates the conditional expectation (2), which is the optimal prediction of the target process X with respect to the L^2-norm. Therefore, we define a new objective function, with which we can prove convergence. Let y_{i-} denote the output of the NJ-ODE at t_i before the jump and y_i the output at t_i after the jump. We remark that the outputs depend on parameters θ and the previously observed x_i which are inputs to the model. Then the objective function is defined as

$$\hat{\Phi}_N(\theta) := \underbrace{\frac{1}{N}\sum_{j=1}^{N}}_{\text{paths}} \underbrace{\frac{1}{n^j}\sum_{i=1}^{n^j}}_{\text{dates}} \Big(\underbrace{|x_i^j - y_i^j|}_{\substack{\text{jump part} \\ \text{at observations}}} + \underbrace{|y_i^j - y_{i-}^j|}_{\substack{\text{continuous part} \\ \text{between two observations}}} \Big)^2. \tag{8}$$

We give an intuitive explanation for this definition. The "jump part" of the loss function forces the JumpNN to produce good updates based on new observations, while the other part forces the jump size to be small in (the empirical) L^2-norm. Since the conditional expectation minimizes the jump size with respect to the L^2-norm, this forces the neural ODE f_θ to continuously transform the hidden state such that the output approximates the conditional expectation. Moreover, both parts of the loss function force the outputNN to reasonably transform the hidden state h_t to the output y_t.

5 Main result – theoretical convergence guarantee

In the following we informally state our main result. To formally state and prove the theorem, precise definitions of all ingredients are needed. This analysis is provided in the appendix where the following results is stated in Theorem E.2 and Theorem E.12.

Theorem 5.1 (informal). *We assume that for each N and for every size of the neural networks, their weights are chosen optimally, as to minimize $\hat{\Phi}_N(\theta)$. Then, if the number of paths and the size of the neural networks tend to infinity, the output of our model converges in mean (L^1-convergence) to the conditional exception of the stochastic process X given the current information.*

An intuitive explanation for this theorem was given with the definition of the objective function. In this result, the focus lies on the convergence analysis under the assumption that optimal weights are found. In the Appendix we discuss, why this assumption is not restrictive.

6 EXPERIMENTS

For further details and results for all experiments see Appendix F.

6.1 TRAINING ON SYNTHETIC DATASETS

Evaluation metric. For synthetic datasets where an analytic formula for the conditional expectation exists, we can evaluate the distance of the model output to the target process (2). We use a sampling time grid with equidistant step size $\Delta_t := \frac{T}{K}$, $K \in \mathbb{N}$, on $[0, T]$. On this grid, we compare for path j at time t, the true conditional expectation $\hat{x}_t^j$ with the predicted conditional expectation (the model output) y_t^j. For N_2 test samples, the evaluation metric is defined as

$$\text{eval}(\hat{x}, y) := \frac{1}{N_2} \sum_{j=1}^{N_2} \frac{1}{K+1} \sum_{i=0}^{K} \left(\hat{x}_{i\Delta_t}^j - y_{i\Delta_t}^j \right)^2 . \tag{9}$$

Black-Scholes, Ornstein-Uhlenbeck and Heston. We test our algorithm on three scalar stochastic models, Black-Scholes, Ornstein-Uhlenbeck and Heston, with fixed parameters. For each model, we generate a dataset by sampling $N = 20'000$ paths on the time interval $[0, 1]$ using the Euler-scheme with 100 time steps. Independently for each path, on average 10% of the grid points are randomly chosen as observation times. The NJ-ODE is trained on 80% of the data. On the remaining 20% the model is tested, by comparing the loss function (32) computed with the NJ-ODE to the loss function computed with the true conditional expectation (Figure 2). During training, the relative difference becomes very small, hence the true conditional expectation is nearly replicated.

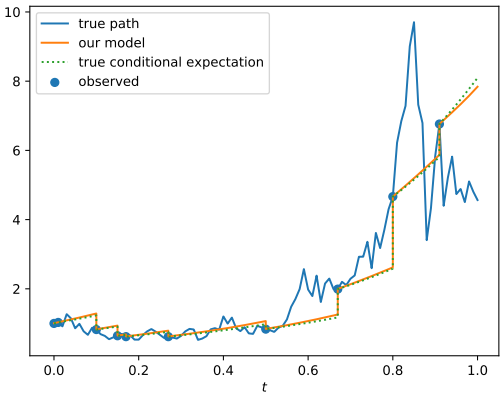

Figure 1: Predicted and true conditional expectation on a test sample of the Heston dataset.

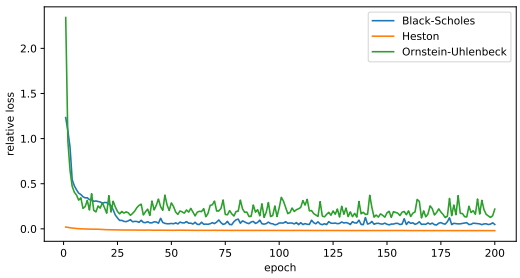

Figure 2: The relative difference between the loss function computed with the predicted conditional expectation and the loss function computed with the true conditional expectation is shown with respect to the number of epochs.

6.2 FURTHER SYNTHETIC DATASETS

Heston model without Feller condition. We also train our model on a Heston dataset for which the Feller condition is not satisfied. As explained by Andersen (2007); Jean-François et al. (2015) this is a more delicate situation. We see that our model is very robust, since even in this delicate case our model learns to replicate the true conditional expectation process. In the Heston model, the variance of the stochastic process X_t is also modelled by a stochastic process v_t. Here, we train our model to predict both processes at the same time. The training on this 2-dimensional dataset is successful as can be seen in Figure 3. The minimal evaluation metric after 200 epochs is 0.0983.

Dataset with changing regime. In this experiment we test, how well our model can deal with stochastic processes, that undergo an (abrupt) change of regime at a certain point in time. Many real world time series might exhibit such a change of regime. Some examples are listed below.

- Longitudinal patient health recordings might experience changes depending on seasonal or longer-term influences, as for example due to the seasonal flue or currently the Covid-19 pandemic.

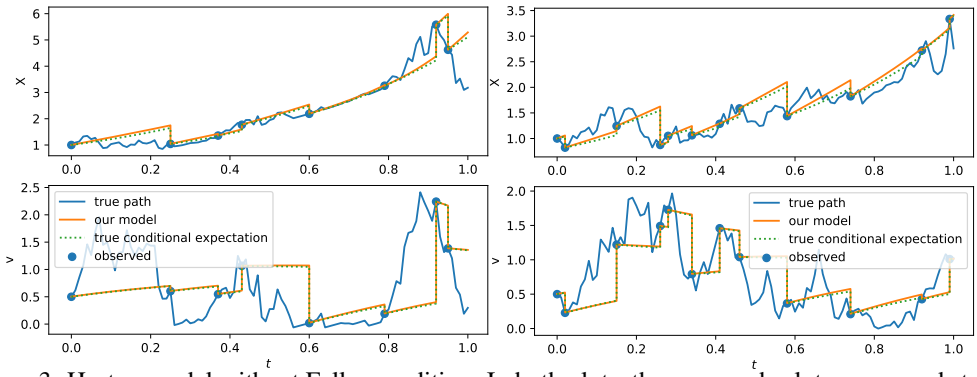

Figure 3: Heston model without Feller condition. In both plots, the upper sub-plot corresponds to the 1-dimensional path of X_t and the lower sub-plot corresponds to the 1-dimensional path of v_t.

- In many regions climate data has strong seasonal dependencies, that can lead to relatively abrupt changes as for example when the weather changes from dry to rain season.
- A stock market that suddenly changes from a bullish to a bearish market, for example due to a macro-economic event. An example for this would be the start of the Covid-19 crisis in the first quarter of 2020.

We test a change of regime by combining two synthetic datasets. On the first half of the time interval $[0, 0.5]$ we use the Ornstein-Uhlenbeck and on the second half $[0.5, 1]$ the Black-Scholes model. In Figure 4 we see that our model correctly learns the change of regime. The minimal evaluation metric after 200 epochs is 0.0463.

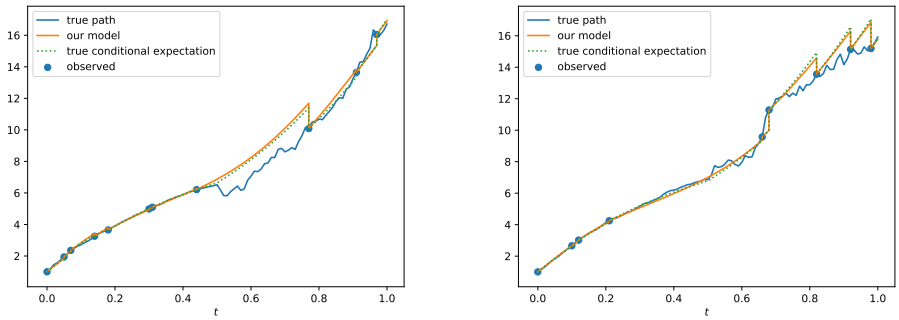

Figure 4: Our model evaluated o a stochastic dataset that follows an Ornstein-Uhlenbeck SDE on the time interval $[0, 0.5]$ and an Black-Scholes model on the time interval $(0.5, 1]$. We see that our model correctly learns the change of regime.

Dataset with explicit time dependence. Many real world datasets, have an explicit time dependence, i.e. the drift and diffusion of (10) explicitly depend on t. Examples are all datasets that have a certain periodicity, as for example weather data (seasonal and daily periodicity), intraday periodicity of stock prices (Andersen & Bollerslev, 1997) or prices of certain seasonal goods. We incorporate an explicit time dependence into the Black-Scholes dataset, by replacing the drift constant μ with the time dependent constant $\frac{\alpha}{2}(\sin(\beta t) + 1)$, for $\alpha, \beta > 0$. In Figure 5 we see that the model learns to adapt to the time-dependent coefficients. The minimal evaluation metric after 100 epochs is 0.0215 ($\beta = 2\pi$) and 0.02805 ($\beta = 4\pi$) respectively.

6.3 Empirical convergence study

We confirm the theoretical results of Theorem 5.1 by an empirical convergence study for growing numbers of training samples N and network size M, where the performance is measured by the evaluation metric (9). For each combination of the number of training samples N_1 and the neural network size M, the NJ-ODE is trained 5 times on the Black-Scholes, Ornstein-Uhlenbeck and

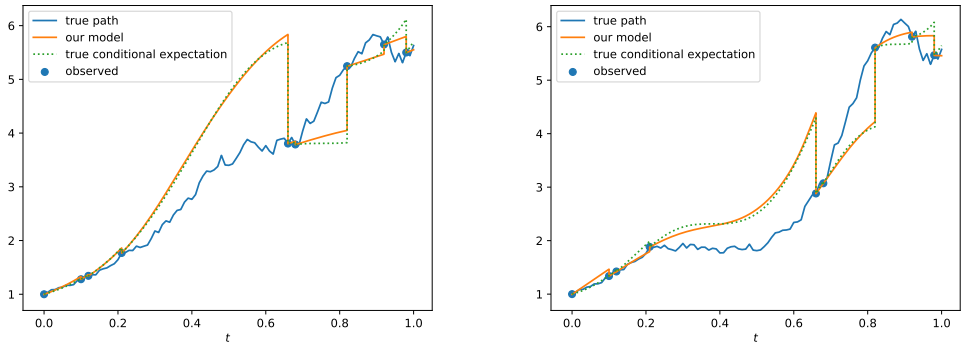

Figure 5: NJ-ODE evaluated on the time-dependent Black-Scholes dataset with $\beta = 2\pi$ (left) and $\beta = 4\pi$ (right).

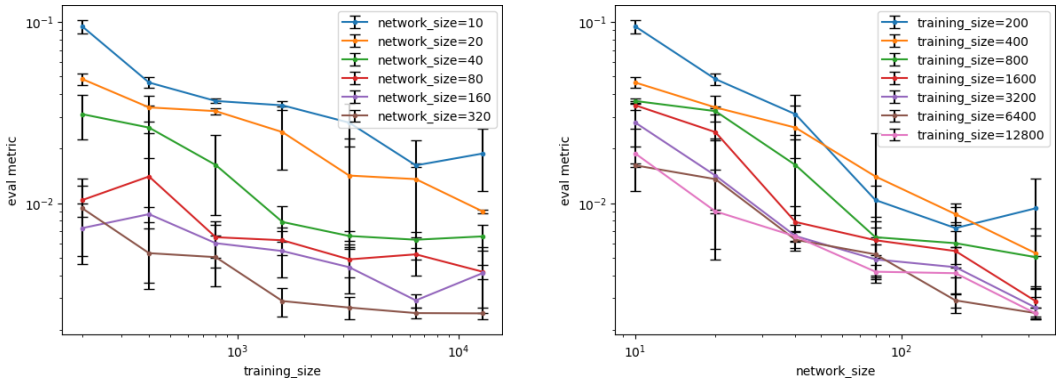

Figure 6: Black-Scholes dataset. Mean $\pm$ standard deviation (black bars) of the evaluation metric for varying training samples N_1 and network size M.

Heston datasets. The means of the evaluation metric over the 5 trials with their standard deviations are shown in Figure 6 for Black-Scholes. Already 200 training samples lead to a small evaluation metric if the network size is big enough, suggesting that the Monte Carlo approximation of the loss function is good, already with a few samples.

6.4 Comparison to GRU-ODE-Bayes on synthetic data

On the Black-Scholes, Ornstein-Uhlenbeck and Heston datasets, we compare our model to GRU-ODE-Bayes (Brouwer et al., 2019), which is, to the best of our knowledge, the neural network based method with the most similar task to ours. Results of our comparison are shown in Table 6.4. On the Black-Scholes and Ornstein-Uhlenbeck dataset, our model performs similarly to GRU-ODE-Bayes. However, on the more complicated Heston dataset, the training of GRU-ODE-Bayes is unstable and does not converge. On the other hand, our model converges during training. Although the value of the evaluation metric is much higher than for Black-Scholes and Ornstein-Uhlebeck, the resulting model output is still meaningful, which is not the case for GRU-ODE-Bayes. Hence we conclude, that GRU-ODE-Bayes cannot be applied reasonably for the Heston dataset, while our method works as the theoretical results suggest.

6.5 Real world datasets with incomplete observations

Self-imputation for incomplete observations. Until now we assumed that at each observation time all coordinates of the stochastic process X are observed. However, in many real world applications, the observations are incomplete, i.e. only for some of the coordinates an observation is available. To deal with such incomplete observations, we propose the following self-imputation method. Whenever an observation $x_i \in \mathbb{R}^{d_X}$ is made the mask $m_i \in \{0,1\}^{d_X}$ tells whether the j-th coordinate of x_i is

Table 1: The minimal, last and average value of the evaluation metric throughout the 100 epochs of training are shown for GRU-ODE-Bayes and our method, together with the number of trainable parameters.

	Black-Scholes		Ornstein-Uhlenbeck		Heston	
	GRU	ours	GRU	ours	GRU	ours
min	$7 \cdot 10^{-4}$	$7 \cdot 10^{-4}$	$3 \cdot 10^{-5}$	$5 \cdot 10^{-4}$	4.24	1.33
last	$3 \cdot 10^{-3}$	$8 \cdot 10^{-3}$	$1 \cdot 10^{-4}$	$6 \cdot 10^{-4}$	30.9	1.35
average	$3 \cdot 10^{-3}$	$1 \cdot 10^{-2}$	$7 \cdot 10^{-4}$	$8 \cdot 10^{-4}$	56.2	1.65
params	$112'602$	$10'071$	$112'602$	$10'071$	$112'602$	$10'071$

observed ($m_i^j = 1$) or not ($m_i^j = 0$). Then we use the prediction y_{i-} of our model to generate the imputed observation vector

$$\tilde{x}_i := m_t \odot x_i + (\mathbf{1}_{d_X} - m_i) \odot y_{i-},$$

where $\odot$ is the element-wise multiplication (Hadamar product) and $\mathbf{1}_{d_X} \in \mathbb{R}^{d_X}$ is the one-vector. Instead of x_i we use $(\tilde{x}_i, m_i)$ as an input for the jump part jumpNN. The intuition behind this definition is the following. In the one dimensional case, if we do not make an observation, but input y_{t-} as if it was an observation, we expect that this does not change the output y_s for $s \geq t$. From this point of view, y_{t-} does not provide any additional information for the model. Similarly, we expect that imputing y_{t-} for unobserved coordinates does not provide any information about this coordinate to the model. However, since the model might learn to transfer the information about an observed coordinate to an unobserved one, we extend the input to also include the information which coordinates were observed. For the ODE part, we use y_i, which is the prediction after processing the input $\tilde{x}_i$, as input instead of x_i. Here, the intuition is that if the model learns how to best use the incomplete observation, i.e. if the jump is good, then this is the best approximation for x_i. Our objective function is adjusted by multiply each term in the sum with the mask.

Climate forecast. We compare our model to GRU-ODE-Bayes on the USHCN daily dataset (Menne et al., 2016), using the same experimental setting as was used by Brouwer et al. (2019). We train a small (S) and a large (L) version of NJ-ODE with different total number of parameters. The validation set was used for early stopping after the first 100 epochs, where we trained for a total of 200 epochs. We see in Table 6.5 that our small version performs slightly worse than GRU-ODE-Bayes while our large version slightly outperforms it.

Table 2: Mean and standard deviation of MSE on the test sets of USHCN. Result of baselines were reported by Brouwer et al. (2019). Where known, the number of trainable parameters is reported.

	USHCN – MSE	# params
neural ODE-VAE	0.96 ± 0.11	-
neural ODE-VAE-MASK	0.83 ± 0.10	-
sequential VAE	0.83 ± 0.07	-
GRU-SIMPLE	0.75 ± 0.12	-
GRU-D	0.53 ± 0.06	-
T-LSTM	0.59 ± 0.11	-
GRU-ODE-Bayes	0.43 ± 0.07	$42'640$
NJ-ODE (S)	0.45 ± 0.06	$10'925$
NJ-ODE (L)	$\mathbf{0.40 \pm 0.07}$	$571'305$

Physionet. We compare our model to the latent ODE on their extrapolation task on the PhysioNet Challenge 2012 dataset (Goldberger et al., 2000), using the same experimental setting as was used by Rubanova et al. (2019). The mean and standard deviation over 5 runs starting at different random initializations is reported for our model. We see in Table 6.5 that our model outperforms the latent ODE models although having only about a seventh of the trainable weights.

Table 3: Mean and standard deviation of MSE on the test set of physionet. Result of baselines were reported by Rubanova et al. (2019). Where known, the number of trainable parameters is reported.

	Physionet – MSE $(\times 10^{-3})$	# params
RNN-VAE	3.055 ± 0.145	-
Latent ODE (RNN enc.)	3.162 ± 0.052	-
Latent ODE (ODE enc)	2.231 ± 0.029	$163'972$
Latent ODE + Poisson	2.208 ± 0.050	$181'723$
NJ-ODE	$\mathbf{1.945 \pm 0.007}$	$24'423$

7 Related work

Stochastic filtering theory. Our main theorem is similar to the theoretical results of *neural filtering* (Lo, 2009), which is a neural network approach to stochastic filtering theory in discrete time. In stochastic filtering, potentially incomplete and noisy observations of X are available continuously in time. This observation process Y is usually described by the dynamics $dY_t = h(X_t)dt + dB_t$, where h is a measurable function and B is a Brownian motion. Stochastic filtering then estimates the conditional law of X_t given the noisy observations $(Y_s)_{0 \leq s \leq t}$ (Bain & Crisan, 2008, Def. 3.2) and therefore can provide conditional expectations. Comparably, we directly compute the conditional expectation given the last observation. Similar to our assumptions, in the neural filtering approach of GRU-ODE-Bayes (Brouwer et al., 2019) and (Ryder et al., 2018) observations are only available at irregular discrete time points. They approximate the conditional law of X given the last observation by a Gaussian distribution and learn its mean and variance parameters. In particular, the conditional expectation is then given by this mean parameter. In contrast, we do not make normality assumptions about the conditional distribution and we theoretically prove convergence to the true conditional expectation.

Neural ODEs with jumps. Except for GRU-ODE-Bayes (Brouwer et al., 2019) and ODE-RNN (Rubanova et al., 2019) another work studying a neural ODE with jumps is *neural jump SDE* (NJSDE) (Jia & Benson, 2019). Similar to the NJ-ODE framework (30), the latent process of NJSDE is described by a neural ODE with jumps at random times. This model is used to describe hybrid systems which evolve continuously in time but may also be interrupted by stochastic events. In contrast to that, we model the conditional expectation of a continuous stochastic process.

8 Conclusion

We presented the neural jump ODE, a data-driven framework for modelling the conditional expectation of a stochastic process given the previous observations. We introduced a rigorous mathematical description of our model and more generally for the class of neural ODE based models. Moreover, this is the first time that for a model falling in this category theoretical guarantees are given. We evaluated our model empirically on six synthetic and two real world datasets. In comparison to the baselines GRU-ODE-Bayes and latent ODE, we achieved better results especially on complex datasets.

References

Leif Andersen. Efficient simulation of the heston stochastic volatility model. *Risk Management*, 2007.

Torben G. Andersen and Tim Bollerslev. Intraday periodicity and volatility persistence in financial markets. *Journal of Empirical Finance*, 1997.

Alan Bain and Dan Crisan. Fundamentals of stochastic filtering. *Springer Science & Business Media*, 60, 2008.

Edward De Brouwer, Jaak Simm, Adam Arany, and Yves Moreau. Gru-ode-bayes: Continuous modeling of sporadically-observed time series. In *NeurIPS*, 2019.

Ricky T. Q. Chen, Yulia Rubanova, Jesse Bettencourt, and David Duvenaud. Neural ordinary differential equations. *NeurIPS*, 2018.

Samuel N Cohen and Robert James Elliott. Stochastic calculus and applications. *Springer*, 2015.

Christa Cuchiero, Martin Larsson, and Josef Teichmann. Deep neural networks, generic universal interpolation, and controlled ODEs. *arxiv:1908.07838*, 2019.

Rick Durrett. Probability: Theory and Examples. *Cambridge University Press*, 2010.

Soheil Feizi, Hamid Javadi, Jesse Zhang, and David Tse. Porcupine neural networks: (almost) all local optima are global. *arXiv:1710.02196*, 2017.

Ary L. Goldberger, Luis A. N. Amaral, Leon Glass, Jeffrey M. Hausdorff, Plamen Ch. Ivanov, Roger G. Mark, Joseph E. Mietus, George B. Moody, Chung-Kang Peng, and H. Eugene Stanley. Physiobank, physiotoolkit, and physionet. *Circulation*, 2000.

Massimiliano Gubinelli. Stochastic analysis - course note 4. *Lecture Notes* https://www.iam.uni-bonn.de/fileadmin/user_upload/gubinelli/stochastic-analysis-ss16/sa-note-4.pdf, 2016.

Calypso Herrera, Florian Krach, and Josef Teichmann. Estimating full lipschitz constants of deep neural networks. *arXiv:2004.13135*, 2020.

Kurt Hornik, Maxwell Stinchcombe, and Halbert White. Multilayer feedforward networks are universal approximators. *Neural Networks*, 2, 1989.

Bégin Jean-François, Bédard Mylène, and Gaillardetz Patrice. Simulating from the heston model: A gamma approximation scheme. *Monte Carlo Methods and Applications*, 2015.

Junteng Jia and Austin R Benson. Neural jump stochastic differential equations. *NeurIPS*, 2019.

Diederik Kingma and Jimmy Ba. Adam: A method for stochastic optimization. *International Conference on Learning Representations*, 2014.

Bernard Lapeyre and Jérôme Lelong. Neural network regression for bermudan option pricing. *arXiv:1907.06474*, 2019.

Andrea Lecchini-Visintini, John Lygeros, and Jan Maciejowski. Simulated annealing: Rigorous finite-time guarantees for optimization on continuous domains. *Advances in Neural Information Processing Systems*, 2008.

Michel Ledoux and Michel Talagrand. Probability in banach spaces. *Springer-Verlag*, 62:67–69, 1991.

Xuechen Li, Ting-Kam Leonard Wong, Ricky T. Q. Chen, and David Duvenaud. Scalable gradients for stochastic differential equations. *arXiv:2001.01328*, 2020.

J. Ting-Ho Lo. Neural Filtering. *Scholarpedia*, 4, 2009.

Marco Locatelli. Simulated annealing algorithms for continuous global optimization: convergence conditions. *Journal of Optimization Theory and applications*, 2000.

M. J. Menne, C. N. Williams, Jr., and R. S. Vose. Long-term daily and monthly climate records from stations across the contiguous united states (u.s.historical climatology network). 2016.

Philip Protter. Stochastic integration and differential equations. *Springer-Verlag*, 2005.

Yulia Rubanova, Ricky T. Q. Chen, and David K Duvenaud. Latent ordinary differential equations for irregularly-sampled time series. In *NeurIPS*. 2019.

Reuven Y Rubinstein and Alexander Shapiro. Discrete event systems: Sensitivity analysis and stochastic optimization by the score function method. *Wiley*, 1993.

Sanae Rujivan and Song-Ping Zhu. A simplified analytical approach for pricing discretely-sampled variance swaps with stochastic volatility. *Applied Mathematics Letters*, 2012.

Thomas Ryder, Andrew Golightly, A. Stephen McGough, and Dennis Prangle. Black-box variational inference for stochastic differential equations. In *ICML*, 2018.

Belinda Tzen and Maxim Raginsky. Neural stochastic differential equations: Deep latent gaussian models in the diffusion limit. *arXiv:1905.09883*, 2019.

Boxuan Yue, Junwei Fu, and Jun Liang. Residual recurrent neural networks for learning sequential representations. *Information*, 9, 2018.

APPENDIX

A SETUP

A.1 STOCHASTIC PROCESS X

In this section in rigorously describe the process X and give the assumptions which are needed in order to derive the convergence results. Let $d_X, d_W \in \mathbb{N}$ and $T > 0$ be the fixed time horizon. Consider a filtered probability space $(\Omega, \mathcal{F}, \mathbb{F} := \{\mathcal{F}_t\}_{0 \leq t \leq T}, \mathbb{P})$, on which an adapted d_W-dimensional Brownian motion $\{W_t\}_{t \in [0,T]}$ is defined. We define the stochastic process[1] $X := (X_t)_{t \in [0,T]}$ as the solution of the stochastic differential equation (SDE)

$$dX_t = \mu(t, X_t)dt + \sigma(t, X_t)dW_t \,, \tag{10}$$

for all $0 \leq t \leq T$, where $X_0 = x \in \mathbb{R}^{d_X}$ is the starting point and the measurable functions $\mu : [0,T] \times \mathbb{R}^{d_X} \to \mathbb{R}^{d_X}$ and $\sigma : [0,T] \times \mathbb{R}^{d_X} \to \mathbb{R}^{d_X \times d_W}$ are the *drift* and the *diffusion* respectively. We impose the following assumptions:

- X **is continuous and square integrable**, i.e. for $\mathbb{P}$-a.e. $\omega \in \Omega$ the map $t \mapsto X_t(\omega)$ is continuous and $\mathbb{E}[X_t^2] < \infty$ for every $t \in [0,T]$.
- μ **and** σ **are both globally Lipschitz continuous in their second component**, i.e. for $\varphi \in \{\mu, \sigma\}$ there exists a constant $M > 0$ such that for all $t \in [0,T]$

$$|\varphi(t,x) - \varphi(t,y)|_2 \leq M|x-y|_2 \quad \text{and} \quad |\varphi(t,x)|_2 \leq (1 + |x|_2)M. \tag{11}$$

  In particular, their growth is at most linear in the second component.
- μ **is bounded and continuous in its first component** (t) **uniformly in its second component** (x), i.e. for every $t \in [0,T]$ and $\varepsilon > 0$ there exists a $\delta > 0$ such that for all $s \in [0,T]$ with $|t-s| < \delta$ and all $x \in \mathbb{R}^{d_X}$ we have $|\mu(t,x) - \mu(s,x)| < \epsilon$.
- σ **is càdlàg** (right-continuous with existing left-limit) **in the first component and** L^2 **integrable with respect to** W**,** $\sigma \in L^2(W)$, i.e

$$\mathbb{E}\left[\sum_{i=1}^{d_X}\sum_{j=1}^{d_W}\int_0^T \sup_x \sigma_{i,j}(x,t)^2 d[W^j, W^j]_t\right] = \int_0^T |\sup_x \sigma(x,t)|_F^2 \, dt < \infty, \tag{12}$$

  where $|\cdot|_F$ denotes the Frobenius matrix norm. This is in particular implied if σ is bounded.

A.2 RANDOM OBSERVATION DATES

In this section we describe how we model the observation dates. We want to treat irregularly observed time-series, i.e. without a fixed number of observations and not necessarily equally distributed. Therefore, we suppose that we have a possibly random number of n observations and that those observations are made at random times $t_1, \ldots, t_n$. For simplicity we make the assumption that the observation dates are independent of the stochastic process itself. In future work, this will be generalized to observation dates correlated with X, that could be modelled by a point process on the same probability space. In contrast, here we hard-code the independence assumption by considering a second probability space $(\tilde{\Omega}, \tilde{\mathcal{F}}, \tilde{\mathbb{P}})$, on which the random observation times of the stochastic process X are defined. More precisely, we assume that:

- $n : \tilde{\Omega} \to \mathbb{N}_{\geq 0}$ is a random variable with $\mathbb{E}_{\tilde{\mathbb{P}}}[n] < \infty$, the random number of observations.
- $t_i : \tilde{\Omega} \to [0,T]$ for $0 \leq i \leq n$ are *sorted* [2] random variables, the random observation times.

We denote the joint pushforward measure of n and $\{t_i\}_{0 \leq i \leq n}$ as $\tilde{\mathbb{P}}_t := (n, t_0, \ldots, t_n)\#\tilde{\mathbb{P}}$. The random variable n can but does not have to be unbounded. If it is bounded, we define $K :=$

[1] A stochastic process is a collection of random variables $X_t : \Omega \to \mathbb{R}^{d_X}, \omega \mapsto X_t(\omega)$ for $0 \leq t \leq T$.

[2] For all $\tilde{\omega} \in \tilde{\Omega}$, $0 = t_0 < t_1(\tilde{\omega}) < \cdots < t_{n(\tilde{\omega})}(\tilde{\omega}) \leq T$.

$\max\left\{k \in \mathbb{N} \,|\, \tilde{\mathbb{P}}(n \geq k) > 0\right\}$ to be the maximal value of n, which otherwise is infinity. We use the notation $\mathcal{B}([0,T])$ for the Borel σ-algebra of the set $[0,T]$. Then we define for each $1 \leq k < K+1$

$$\lambda_k : \mathcal{B}([0,T]) \to [0,1], \quad B \mapsto \lambda_k(B) := \frac{\tilde{\mathbb{P}}(n \geq k, (t_k-) \in B)}{\tilde{\mathbb{P}}(n \geq k)},$$

which is a probability measure on the time interval as shown in the lemma below. Here, (t_k-) means the left-point of t_k, for example, if $t_0 = 0, t_1 = 1$ we have $t_0 \in [0,1), t_1 \notin [0,1)$ but $t_0- \notin [0,1), t_1- \in [0,1)$.

Lemma A.1. *For $1 \leq k < K+1$ the map λ_k defines a probability measure.*

Proof. First we see that $\lambda_k([0,T]) = 1$ since t_k maps to $[0,T]$. Furthermore, for any disjoint sets $B_i \in \mathcal{B}([0,T])$, $i \in \mathbb{N}$, we have $\{n \geq k, t_k- \in \dot{\cup}_{i\geq 1} B_i\} = \dot{\cup}_{i \geq 1}\{n \geq k, t_k- \in B_i\}$ and these sets are $\tilde{\mathcal{F}}$-measurable, since they are defined through pre-images of random variables. Therefore, the additivity of $\tilde{\mathbb{P}}$ implies that $\lambda_k\left(\dot{\cup}_{i\geq 1} B_i\right) = \sum_{i \geq 1} \lambda_k\left(B_i\right)$. □

Moreover, we define τ as the time of the last observation before a certain time t,

$$\tau : [0,T] \times \tilde{\Omega} \to [0,T], \quad (t, \tilde{\omega}) \mapsto \tau(t, \tilde{\omega}) := \max\{t_i(\tilde{\omega}) | 0 \leq i \leq n(\tilde{\omega}), t_i(\tilde{\omega}) \leq t\}.$$

Example A.2. *We give two examples how the random observation dates could be defined.*

- *Let $(N_t)_{t\in[0,T]}$ be a homogeneous Poisson point process with rate $r > 0$. Hence, $N(0) = 0$, $t \mapsto N(t)$ is constant except for jumps of size 1 at discrete random times and for any fixed $t \in [0,T]$, $N(t)$ is Poisson distributed, i.e.*

  $$\tilde{\mathbb{P}}[N(t) = k] = \frac{(rt)^k}{k!} e^{-rt} \text{ for } k \in \mathbb{N}.$$

  Then the number of observations is defined as $n := N(T)$ and satisfies $\mathbb{E}_{\tilde{\mathbb{P}}}[n] = rT$. The observation dates $t_1, \ldots, t_n$ are defined as the discontinuity times of N, i.e. the times where N increases by 1. In particular, for $0 \leq k \leq n$, $t_k := \inf\{t | N(t) = k\} \leq T$. Therefore, for $0 \leq a \leq b \leq T$ we can rewrite

  $$\lambda_k((a,b)) = \frac{\tilde{\mathbb{P}}(N(a) < k, N(b) \geq k)}{\tilde{\mathbb{P}}(N(T) \geq k)}.$$

- *We define n by one of the following options:*
  - *as a constant in $\mathbb{N}_{>0}$.*
  - *as a Binomial random variable, $n \sim \mathrm{Binom}(p, n_{\max})$, for $p \in (0,1)$, $n_max \in \mathbb{N}_{>0}$.*
  - *as a Geometric random variable, $n \sim \mathrm{Geom}(p)$, for $p \in (0,1)$.*
  - *as a Poisson random variable, $n \sim \mathrm{Poi}(r)$, for $r > 0$.*

  and $t_1, \ldots, t_n$ are defined by choosing n uniform random variables on $[0,T]$ and sorting them.

A.3 Information σ-algebra

In this section, we define a mathematical tool, the σ-algebra, that is essential to the description of the conditional expectation. This object describes which information is available at a certain time t. In the following, we leave away $\tilde{\omega} \in \tilde{\Omega}$ whenever the meaning is clear. We define the filtration of the currently available information $\mathbb{A} := (\mathcal{A}_t)_{t\in[0,T]}$ by

$$\mathcal{A}_t := \boldsymbol{\sigma}(X_{t_i} | t_i \leq t),$$

where t_i are the observation times and $\boldsymbol{\sigma}(\cdot)$ denotes the generated σ-algebra. By the definition of τ we have $\mathcal{A}_t = \mathcal{A}_{\tau(t)}$ for all $t \in [0,T]$. $(\Omega \times \tilde{\Omega}, \mathcal{F} \otimes \tilde{\mathcal{F}}, \mathbb{F} \otimes \tilde{\mathcal{F}}, \mathbb{P} \times \tilde{\mathbb{P}})$ is the filtered product probability space which, intuitively speaking, combines the randomness of the stochastic process with the randomness of the observations. Here, $\mathbb{F} \otimes \tilde{\mathcal{F}}$ consists of the tensor-product σ-algebras $(\mathcal{F} \otimes \tilde{\mathcal{F}})_t := \mathcal{F}_t \otimes \tilde{\mathcal{F}}$ for $t \in [0,T]$. As explained in the remark below, $\mathcal{A}_t$ can be identified with a sub-σ-algebra of $(\mathcal{F} \otimes \tilde{\mathcal{F}})_t$.

Remark A.3. *The σ-fields $\mathcal{A}_t$ depend on $\tilde{\omega} \in \tilde{\Omega}$ as well. If we look at the product probability space $(\Omega \times \tilde{\Omega}, \mathcal{F} \otimes \tilde{\mathcal{F}}, \mathbb{F} \otimes \tilde{\mathcal{F}}, \mathbb{P} \times \tilde{\mathbb{P}})$, where $\mathbb{F} \otimes \tilde{\mathcal{F}}$ consists of the tensor-product σ-algebras $(\mathcal{F} \otimes \tilde{\mathcal{F}})_t := \mathcal{F}_t \otimes \tilde{\mathcal{F}}$ for $t \in [0, T]$, then*

$$\begin{aligned}&\boldsymbol{\sigma}(X_{t_i} | t_i \leq t)\\ &\quad := \boldsymbol{\sigma}\left(\left\{\left\{(\omega, \tilde{\omega}) \in \Omega \times \tilde{\Omega} \middle| X_{t_i(\tilde{\omega})}(\omega) \in A, n(\tilde{\omega}) \geq i, t_i(\tilde{\omega}) \leq t\right\} \middle| A \in \mathcal{B}(\mathbb{R}^{d_X}), i \in \mathbb{N}\right\}\right)\end{aligned}$$

is a well defined sub-σ-algebra of $(\mathcal{F} \otimes \tilde{\mathcal{F}})_t$. Furthermore, we can recover the $\tilde{\omega}$-wise defined version of $\mathcal{A}_t$ by intersecting each set in it with $\Omega \times \{\tilde{\omega}\}$ and subsequently projecting the intersection on its first component. We use the notation $\tilde{\mathcal{A}}_t := \tilde{\mathcal{A}}_t(\tilde{\omega}) = \boldsymbol{\sigma}(X_{t_i(\tilde{\omega})} | t_i(\tilde{\omega}) \leq t)$ to distinguish this $\tilde{\omega}$-wise definition from the definition as sub-σ-algebra of the product space given above. However, Lemma B.3 implies that for our considerations, both versions of this σ-algebra have the same effect, therefore we will simply write $\mathcal{A}_t$ for both versions, by abuse of notation.

B Optimal approximation $\hat{X}$ of the stochastic process X

We are interested in the "best" approximation (or prediction) $\hat{X}_t$ of the process X that one can make at any time $t \in [0, T]$, given the currently available information $\mathcal{A}_t$. For us "best" refers to the $L^2(\Omega \times \tilde{\Omega}, \mathbb{F} \otimes \tilde{\mathcal{F}}, \mathbb{P} \times \tilde{\mathbb{P}})$-minimizer, therefore, this approximation is given by the conditional expectation. Indeed, if we define $\Delta := \{(t, r) \in [0, T]^2 | t + r \leq T\}$, and the function

$$\tilde{\mu} : \Delta \times \mathbb{R}^{d_X} \to \mathbb{R}^{d_X}, \quad ((t, r), \xi) \mapsto \mathbb{E}\left[\mu(t + r, X_{t+r}) | X_t = \xi\right],$$

this is proven in the following proposition.

Proposition B.1. *The optimal (i.e. L^2-norm minimizing) $\mathbb{A}$-adapted process in $L^2(\Omega \times \tilde{\Omega}, \mathbb{F} \otimes \tilde{\mathcal{F}}, \mathbb{P} \times \tilde{\mathbb{P}})$ approximating $(X_t)_{t \in [0,T]}$ is given by[3] $\hat{X} := (\hat{X}_t)_{t \in [0,T]}$ with $\hat{X}_t := \mathbb{E}_{\mathbb{P} \times \tilde{\mathbb{P}}}[X_t | \mathcal{A}_t]$. Moreover, this process is unique up to $(\mathbb{P} \times \tilde{\mathbb{P}})$-null-sets. In addition we have ($\tilde{\omega}$-wise for $\tilde{\omega} \in \tilde{\Omega}$) that*

$$\hat{X}_t = X_{\tau(t)} + \int_{\tau(t)}^{t} \tilde{\mu}\left(\tau(t), s - \tau(t), X_{\tau(t)}\right) ds, \tag{13}$$

implying that $\hat{X}$ is càdlàg.

The first part of the result follows from the elementary Proposition below (which is proven for example in (Durrett, 2010, Thm. 5.1.8) for $\mathbb{R}$-valued random variables and can easily be extended to $\mathbb{R}^d$-valued random variables when using the 2-norm).

Proposition B.2. *Given a probability space $(\Omega, \mathcal{F}, \mathbb{P})$ and a sub-σ-algebra $\mathcal{A} \subset \mathcal{F}$, the orthogonal projection of $X \in L^2(\Omega, \mathcal{F}, \mathbb{P})$ on $L^2(\Omega, \mathcal{A}, \mathbb{P})$ is given by $\hat{X} := \mathbb{E}[X | \mathcal{A}]$. In particular, for every $Z \in L^2(\Omega, \mathcal{A}, \mathbb{P})$ with $\mathbb{P}(Z \neq \hat{X}) > 0$ we have*

$$E[|X - Z|_2^2] = \mathbb{E}[|X - \hat{X}|_2^2] + \mathbb{E}[|Z - \hat{X}|_2^2] > \mathbb{E}[|X - \hat{X}|_2^2].$$

Proof Proposition B.1. In our case this means, that the optimal $\mathbb{A}$-adapted process in $L^2(\Omega \times \tilde{\Omega}, \mathbb{F} \otimes \tilde{\mathcal{F}}, \mathbb{P} \times \tilde{\mathbb{P}})$ approximating X is given by $(\hat{X}_t)_{t \in [0,T]}$ with $\hat{X}_t := \mathbb{E}_{\mathbb{P} \times \tilde{\mathbb{P}}}[X_t | \mathcal{A}_t]$. Here, $\mathcal{A}_t$ is meant as a sub-σ-algebra of $\mathcal{F}_t \times \tilde{\mathcal{F}}$. This process is unique up to $(\mathbb{P} \times \tilde{\mathbb{P}})$-null-sets. Moreover, the following lemma shows that it coincides $\tilde{\omega}$-wise with $\mathbb{E}_{\mathbb{P}}[X_t | \tilde{\mathcal{A}}_t](\tilde{\omega})$, where $\tilde{\mathcal{A}}_t = \tilde{\mathcal{A}}_t(\tilde{\omega})$ is defined in Remark A.3.

Lemma B.3. *For $\tilde{\mathbb{P}}$-almost-every $\tilde{\omega} \in \tilde{\Omega}$ we have $\mathbb{E}_{\mathbb{P} \times \tilde{\mathbb{P}}}[X_t | \mathcal{A}_t](\tilde{\omega}) = \mathbb{E}_{\mathbb{P}}[X_t | \tilde{\mathcal{A}}_t](\tilde{\omega})$ $\mathbb{P}$-almost-surely.*

[3] While we give a pointwise definition, (Cohen & Elliott, 2015, Theorem 7.6.5) allows to define $\hat{X}$ directly as the optional projection. By (Cohen & Elliott, 2015, Remark 7.2.2) this implies that the process $\hat{X}$ is progressively measurable, in particular, jointly measurable in t and $\omega \times \tilde{\omega}$. However, as we show below, even from the pointwise definition, it follows that $\hat{X}$ is càdlàg, hence optional (Cohen & Elliott, 2015, Theorem 7.2.7).

Proof. Otherwise we have by Fubini's theorem, Proposition B.2 and an argument similar to the one in Lemma E.4

$$\mathbb{E}_{\mathbb{P}\times\tilde{\mathbb{P}}}\left[\left|X_t - \mathbb{E}_{\mathbb{P}\times\tilde{\mathbb{P}}}[X_t|\mathcal{A}_t]\right|_2^2\right] = \mathbb{E}_{\tilde{\mathbb{P}}}\left[\mathbb{E}_{\mathbb{P}}\left[\left|X_t - \mathbb{E}_{\mathbb{P}\times\tilde{\mathbb{P}}}[X_t|\mathcal{A}_t]\right|_2^2\right]\right]$$
$$> \mathbb{E}_{\tilde{\mathbb{P}}}\left[\mathbb{E}_{\mathbb{P}}\left[\left|X_t - \mathbb{E}_{\mathbb{P}}[X_t|\tilde{\mathcal{A}}_t]\right|_2^2\right]\right],$$

which is a contradiction to Proposition B.2. □

This proves the first part of Proposition B.1. The second part of this Proposition, i.e. (13), should be understood $\tilde{\omega}$-wise, for $\tilde{\omega} \in \tilde{\Omega}$. This is justified by Lemma B.3 and derived below. In particular, for the remainder of this section, all statements are meant $\tilde{\omega}$-wise.

With the assumption that μ and σ are Lipschitz, (Protter, 2005, Thm. 7, Chap. V) implies that a unique solution of (10) exists. Furthermore, this solution is a Markov process as soon as the starting point x is fixed (Protter, 2005, Thm. 32, Chap. V). Hence, one can define a transition function P (compare (Protter, 2005, Chap. V.6)) such that for all $s < t$ and ϕ bounded and measurable,

$$P_{s,t}(X_s, \phi) := \mathbb{E}[\phi(X_t)|\boldsymbol{\sigma}(X_s)] = \mathbb{E}_{\mathbb{P}}[\phi(X_t)|\mathcal{F}_s].$$

We have that $X_{\tau(s)}$ is $\mathcal{A}_{\tau(s)}$-measurable and therefore, since $\mathcal{A}_s = \mathcal{A}_{\tau(s)} \subset \mathcal{F}_{\tau(s)}$,

$$P_{\tau(s),t}(X_{\tau(s)}, \phi) = \mathbb{E}_{\mathbb{P}}[\phi(X_t)|\mathcal{A}_s]. \tag{14}$$

By our additional assumption on σ it follows from (Protter, 2005, Lem. before Thm. 28, Chap. IV) that

$$M_t := \int_0^t \sigma(s, X_s)dW_s, \quad 0 \le t \le T,$$

is a square integrable martingale, since the Browian motion W is square integrable. In particular, for $0 \le s \le t \le T$ we have $\mathbb{E}[\int_s^t \sigma(r, X_r)dW_r|\mathcal{F}_s] = \mathbb{E}[M_t - M_s|\mathcal{F}_s] = 0$. Moreover, the same is true when conditioning on $\mathcal{A}_s$ [4].

Using the martingale property of M, we have ($\tilde{\omega}$-wise) for every $t \in [0, T]$

$$\begin{aligned}\hat{X}_t &= \mathbb{E}_{\mathbb{P}}[(X_t - X_{\tau(t)}) + X_{\tau(t)}|\mathcal{A}_{\tau(t)}] \\ &= X_{\tau(t)} + \mathbb{E}_{\mathbb{P}}\left[\int_{\tau(t)}^t \mu(r, X_r)dr\Big|\mathcal{A}_{\tau(t)}\right] + \mathbb{E}_{\mathbb{P}}\left[\int_{\tau(t)}^t \sigma(r, X_r)dW_r\Big|\mathcal{A}_{\tau(t)}\right] \\ &= X_{\tau(t)} + \int_{\tau(t)}^t \mathbb{E}_{\mathbb{P}}\left[\mu(r, X_r)|\mathcal{A}_{\tau(t)}\right] dr,\end{aligned} \tag{15}$$

where we used Fubini's Theorem (for conditional expectations) in the last step. This is justified because $\mathbb{E}_{\mathbb{P}}[\int_0^T |\mu(r, X_r)|_2 dr] < \infty$ follows from μ being bounded. Let us define $\Delta := \{(t, r) \in [0, T]^2 | t + r \le T\}$ and the function

$$\tilde{\mu} : \Delta \times \mathbb{R}^{d_X} \to \mathbb{R}^{d_X}, \quad ((t, r), \xi) \mapsto P_{t,t+r}(X_t, \mu)\big|_{X_t=\xi} = \mathbb{E}_{\mathbb{P}}\left[\mu(t + r, X_{t+r})|X_t = \xi\right],$$

then we can use (14) to rewrite (15) as

$$\hat{X}_t = X_{\tau(t)} + \int_{\tau(t)}^t \tilde{\mu}\left(\tau(t), s - \tau(t), X_{\tau(t)}\right) ds. \tag{16}$$

This proves the second part of Proposition B.1. □

Proposition B.4. *The function $\tilde{\mu}$ is (jointly) continuous.*

[4] To see this, we choose a localizing sequence $(\tau_n)_{n\in\mathbb{N}}$ such that M^{τ_n} is bounded by n (works since M is continuous). Then the Markov property implies that $\mathbb{E}[M_t^{\tau_n} - M_s^{\tau_n}|\mathcal{A}_s] = \mathbb{E}[M_t^{\tau_n} - M_s^{\tau_n}|\mathcal{F}_s] = 0$. Since $M_t^{\tau_n} \xrightarrow{n\to\infty} M_t$ $\mathbb{P}$-a.s. and since this sequence is dominated by the integrable random variable $1 + \sup_{r\le t}\|M_r\|^2$ (by Doob's inequality and square integrability of M), dominated convergence implies that $\mathbb{E}[M_t - M_s|\mathcal{A}_s] = 0$.

Proof of Proposition B.4. For any fixed $s \in [0,T], x \in \mathbb{R}^{d_X}$, we define

$$\zeta_{s,\cdot}(x) : [0,T] \times \Omega \to \mathbb{R}^{d_X}, (t,\omega) \mapsto \zeta_{s,t}(x)(\omega)$$

to be the solution of the SDE

$$\zeta_{s,t}(\xi) = \xi + \int_s^t \mu(r, \zeta_{s,r})dr + \int_s^t \sigma(r, \zeta_{s,r})dW_r.$$

This solution exists and is unique by (Protter, 2005, Chap. V, Thm. 7), therefore we have that $X_t = \zeta_{0,t}(x)$ $\mathbb{P}$-almost surely. Furthermore, (Gubinelli, 2016, Thm. 4) implies that for $s \leq t$ we have $X_t = \zeta_{s,t}(\zeta_{0,s}(x))$. Hence, for $t = s + r$, we have the identity $\tilde{\mu}(s, r, \xi) = \mathbb{E}[\mu(t, \zeta_{s,t}(\xi))]$.

Furthermore, by (Gubinelli, 2016, Thm. 8) we have for any $\xi, \xi' \in \mathbb{R}^{d_X}$ and $(s,r), (s',r') \in \Delta$ with $t := s + r, t' := s' + r' \in [0,T]$ that there exists some constant C such that

$$\mathbb{E}\left[|\zeta_{s,t}(\xi) - \zeta_{s',t'}(\xi')|_2^2\right] \leq C\left[|\xi - \xi'|_2^2 + (1 + |\xi|_2 + |\xi'|_2)^2 (|t - t'| + |s - s'|)\right]. \tag{17}$$

Therefore, we have that

$$\begin{aligned}
|\tilde{\mu}(s,r,\xi) - \tilde{\mu}(s',r',\xi')|_2 &= |\mathbb{E}\left[\mu(t, \zeta_{s,t}(\xi))\right] - \mathbb{E}\left[\mu(t', \zeta_{s',t'}(\xi'))\right]|_2 \\
&\leq |\mathbb{E}\left[\mu(t, \zeta_{s,t}(\xi))\right] - \mathbb{E}\left[\mu(t', \zeta_{s,t}(\xi))\right]|_2 \\
&\quad + |\mathbb{E}\left[\mu(t', \zeta_{s,t}(\xi))\right] - \mathbb{E}\left[\mu(t', \zeta_{s',t'}(\xi'))\right]|_2 \\
&\leq \mathbb{E}\left[|\mu(t, \zeta_{s,t}(\xi)) - \mu(t', \zeta_{s,t}(\xi))|_2^2\right]^{1/2} \\
&\quad + \mathbb{E}\left[|\mu(t', \zeta_{s,t}(\xi)) - \mu(t', \zeta_{s',t'}(\xi'))|_2^2\right]^{1/2} \\
&\leq \mathbb{E}\left[|\mu(t, \zeta_{s,t}(\xi)) - \mu(t', \zeta_{s,t}(\xi))|_2^2\right]^{1/2} \\
&\quad + M\,\mathbb{E}\left[|\zeta_{s,t}(\xi) - \zeta_{s',t'}(\xi')|_2^2\right]^{1/2},
\end{aligned} \tag{18}$$

where we used Jensen's inequality in the second last and (11) in the last step. Hence, for $(s', r', \xi') \to (s, r, \xi)$ we have that the first term of (18) goes to zero due to continuity of μ in its first component uniformly in the second component. Moreover, the second term of (18) converges to zero by (17). Together, this proves continuity of $\tilde{\mu}$. □

C Recall: RNN, neural ODE and ODE-RNN - equivalent ways of writing

We describe our model as the solution of the SDE (30), which is a compact way of writing. In the following, we first shortly recall recurrent neural networks (RNN) and the neural ODE and then recall the ODE-RNN. Furthermore, we give a step-by-step explanation, how the way ODE-RNN was formalized, can equivalently be written in terms of an SDE similar to (30). Finally we give the alternative way of writing our model and a short comparison to ODE-RNN.

Recurrent Neural Network. The input to a RNN is a discrete time series of observations $\{x_{t_1}, \cdots, x_{t_n}\}$. At each time t_{i+1}, the latent variable h is updated using the previous latent variable h_{t_i} and the input $x_{t_{i+1}}$ as

$$h_{t_{i+1}} := \text{RNNCell}(h_{t_i}, x_{t_{i+1}}), \tag{19}$$

where RNNCell is a neural network.

Neural Ordinary Differential Equation. Neural ODEs (Chen et al., 2018) are a family of continuous-time models defining a latent variable $h_t := h(t)$ to be the solution to an ODE initial-value problem (IVP):

$$h_t := h_{t_0} + \int_{t_0}^t f(h_s, s, \theta)ds, \quad t \geq t_0, \tag{20}$$

where $f(\cdot, \cdot, \theta) = f_\theta$ is a neural network with weights θ. Therefore, the latent variables can be updated continuously by solving this ODE (20). We can emphasize the dependence of h_t on a numerical ODE solver by rewriting (20) as

$$h_t := \text{ODESolve}(f_\theta, h_{t_0}, (t_0, t)). \tag{21}$$

ODE-RNN. ODE-RNN (Rubanova et al., 2019) is a mixture of a RNN and a neural ODE. In contrast to a standard RNN, we are not only interested in an output at the observation times t_i, but also in between those times. In particular, we want to have an output stream that is generated continuously in time. This is achieved by using a neural ODE to model the latent dynamics between two observation times, i.e. for $t_i < t < t_{i+1}$ the latent variable is defined as in (20) and (21), with h_{t_0} and t_0 replaced by h_{t_i} and t_i. At the next observation time t_{i+1}, the latent variable is then updated by a RNN. Rubanova et al. (2019) write this as

$$\begin{cases} h'_{t_{i+1}} & := & \text{ODESolve}(f_\theta, h_{t_i}, (t_i, t_{i+1})) \\ h_{t_{i+1}} & := & \text{RNNCell}(h'_{t_{i+1}}, x_{t_{i+1}}) \,. \end{cases} \tag{22}$$

Therefore, fixing $h_{t_0} := h_0$, the entire latent process can be computed by iteratively solving an ODE followed by applying a RNN.

GRU-ODE-Bayes. The model architecture describing the latent variable in GRU-ODE-Bayes (Brouwer et al., 2019) is defined as the ODE-RNN but with the special choice of a gated recurrent unit (GRU) for the RNN-cell and the neural network f_θ also being derived from a GRU.

ODE-RNN as càdlàg process. Thinking about the process $h := (h_t)_{t \geq t_0}$ defined in (22) as a (stochastic) process in time, it is defined to evolve continuously for $t_i \leq t < t_{i+1}$ according to the ODE dynamics f_θ and jumps at time t_{i+1} according to the RNN cell. In particular, it is defined to be a *càdlàg*[5] process, for which $h_{t_{i+1}-}$ is the standard notation for the left limit, i.e. the last point before the jump at time t_{i+1}. According to this notation we have $h_{t_{i+1}-} = h'_{t_{i+1}}$, hence, we can rewrite (22) as

$$\begin{cases} h_{t_{i+1}-} & := & \text{ODESolve}(f_\theta, h_{t_i}, (t_i, t_{i+1})) \\ h_{t_{i+1}} & := & \text{RNNCell}(h_{t_{i+1}-}, x_{t_{i+1}}) \,. \end{cases} \tag{23}$$

C.1 Residual ODE-RNN as a special case of controlled ODE

Residual ODE-RNN. We replace the standard RNN cell by a *residual RNN cell* (rRNN), as it was described e.g. in Yue et al. (2018). In particular, instead of applying the RNN cell such that $h_{t_i} = \text{RNNCell}(h_{t_i-}, x_i)$ we use a residual RNN cell to have $h_{t_i} = h_{t_i-} + \text{rRNNCell}(h_{t_i-}, x_i)$. The residual RNN is as expressive as the standard RNN and was empirically shown to perform very similarly or even better than the standard framework (Yue et al., 2018). This way, the residual RNN cell models exactly the jump of the latent variable (i.e. the differences) that occurs at the time t_{i+1} when taking into account the next observation $x_{t_{i+1}}$. Therefore, we can rewrite the ODE-RNN (23) as

$$\begin{cases} h_{t_{i+1}-} & := & \text{ODESolve}(f_\theta, h_{t_i}, (t_i, t_{i+1})) \\ h_{t_{i+1}} & := & h_{t_{i+1}-} + \text{rRNNCell}(h_{t_{i+1}-}, x_i) \,. \end{cases} \tag{24}$$

Controlled Ordinary Differential Equation. We briefly recall the definition of *controlled ODEs* as it was given in (Herrera et al., 2020, Section 4.1) and used in (Cuchiero et al., 2019; Herrera et al., 2020) to describe neural networks. We fix $\ell, d \in \mathbb{N}$ and define for $1 \leq i \leq d$ the vector fields

$$V_i : \Theta \times \mathbb{R}_{\geq 0} \times \mathbb{R}^\ell \to \mathbb{R}^\ell, (\theta, t, x) \mapsto V_i^\theta(t, x),$$

which are càglàd[6] in t and Lipschitz continuous in x. Furthermore, we define the scalar càdlàg *control* functions

$$u_i : \mathbb{R}_{\geq 0} \to \mathbb{R}, t \mapsto u_i(t),$$

which have finite variation and satisfy $u_i(0) = 0$. Then we define the process $Z := (Z_t)_{t \geq 0}$ as the solution of the controlled ODE

$$dZ_t = \sum_{i=1}^{d} V_i^\theta\big(t, Z_{t-}\big) du_i(t), \;\; Z_0 = z, \tag{25}$$

where $z \in \mathbb{R}^\ell$ is some starting point. (25) is written in Itô's differential notation for (stochastic) integrals. The solution of (25) exists and is unique under much more general assumptions than we made here (Protter, 2005, Chap. V, Thm. 7).

[5] i.e. right-continuous with existing left limits, also denoted as *RCLL*

[6] i.e. left continuous with existing right limits

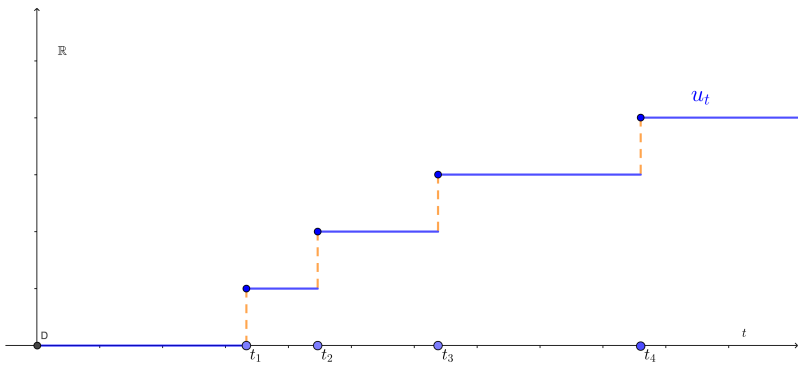

Figure 7: Schematic representation of the stochastic control u_t (26).

Special Case: ODE-RNN. To write the ODE-RNN as controlled ODE, we set $d = 2$ and define $V_1^\theta := f_\theta$, $V_2 :=$ rRNNCell and $u_1(t) := t$. As pointed out by Herrera et al. (2020), one can take the u_i to be semimartingales instead of deterministic functions. In line with this, we define $u_2 := u$ as the pure jump stochastic control process

$$u : \tilde{\Omega} \times [0, T] \to \mathbb{R}, (\tilde{\omega}, t) \mapsto u_t(\tilde{\omega}) := \sum_{i=1}^{n(\tilde{\omega})} \mathbf{1}_{[t_i(\tilde{\omega}),\infty)}(t). \tag{26}$$

We note that u is an adapted process starting at 0 with finite variation on the product probability space $(\Omega \times \tilde{\Omega}, \mathcal{F} \otimes \tilde{\mathcal{F}}, \mathbb{F} \otimes \tilde{\mathcal{F}}, \mathbb{P} \times \tilde{\mathbb{P}})$, since the variation of u up to time T is n and $\mathbb{E}_{\mathbb{P}\times\tilde{\mathbb{P}}}[n] < \infty$. The following result shows that the residual ODE-RNN can compactly be described as a controlled ODE.

Proposition C.1. *Using the vector fields and controls defined above, the latent variable process $h = (h_t)_{t \geq t_0}$ of the residual ODE-RNN can equivalent be written as the solution of the controlled ODE*

$$dh_t = f_\theta(h_{t-}, t-)dt + \text{rRNNCell}(h_{t-}, x_t)du(t), \quad h_{t_0} = h_0. \tag{27}$$

Proof of Proposition C.1. By (Protter, 2005, Chap. II, Thm. 17), the stochastic integral is indistinguishable from the path-wise Lebesgue-Stieltjes integral if the integrator is of finite variation. Hence, we can assume that some $\tilde{\omega} \in \tilde{\Omega}$ is fixed and that the following expressions are evaluated at this $\tilde{\omega}$ whenever applicable. First note, that u is constant except at the t_i where it increases by 1 (cf. Figure 7). In particular, the Lebesgue-Stieltjes integral of some càdlàg function g with respect to u is a sum, i.e. $\int_0^t g(s-)du_s = \sum_{t_i \leq t} g(t_i-)\Delta u_{t_i}$, where $\Delta u_{t_i} = u_{t_i} - u_{t_i-} = 1$. Therefore, integrating (27) from t_0 to t we get

$$\begin{aligned} h_t &= h_{t_0} + \int_{t_0}^t f_\theta(h_{s-}, s-)ds + \int_{t_0}^t \text{rRNNCell}(h_{s-}, x_s)du(s) \\ &= h_{t_0} + \int_{t_0}^t f_\theta(h_{s-}, s-)ds + \sum_{t_i \leq t} \text{rRNNCell}(h_{t_i-}, x_{t_i}). \end{aligned}$$

In particular, since the first integral is continuous in t, we have for every $1 \leq k \leq n$

$$\begin{aligned} h_{t_k} &= h_{t_0} + \int_{t_0}^{t_k-} f_\theta(h_{s-}, s-)ds + \sum_{t_i < t_k} \text{rRNNCell}(h_{t_i-}, x_{t_i}) + \text{rRNNCell}(h_{t_k-}, x_{t_k}) \\ &= h_{t_k-} + \text{rRNNCell}(h_{t_k-}, x_{t_k}), \end{aligned} \tag{28}$$

and for $t_k < t < t_{k+1}$

$$\begin{aligned} h_t &= h_{t_0} + \int_{t_0}^{t_k} f_\theta(h_{s-}, s-)ds + \sum_{t_i \leq t_k} \text{rRNNCell}(h_{t_i-}, x_{t_i}) + \int_{t_k}^t f_\theta(h_{s-}, s-)ds \\ &= h_{t_k} + \int_{t_k}^t f_\theta(h_{s-}, s-)ds. \end{aligned} \tag{29}$$

Together, (28) and (29) prove that (27) is equivalent to (24). We also emphasize that x_t is used as input only for $t = t_i$, $1 \leq i \leq n$. □

D NEURAL JUMP ODE

We propose a model framework whose architecture can be interpreted as a simplification of the ODE-RNN (Rubanova et al., 2019) and the GRU-ODE-Bayes (Brouwer et al., 2019) model architecture.

D.1 THE MODEL FRAMEWORK: NEURAL ODE BETWEEN JUMPS

We define $\mathcal{X} \subset \mathbb{R}^{d_X}$ and $\mathcal{H} \subset \mathbb{R}^{d_H}$ to be the observation and latent space for $d_X, d_H \in \mathbb{N}$. Moreover, we define the following feed-forward neural networks with sigmoid activation functions:

- $f_{\theta_1} : [-1,1]^{d_H} \times [-1,1]^{d_X} \times [0,T] \times [0,T] \to \mathbb{R}^{d_H}$ modelling the ODE dynamics,
- $\rho_{\theta_2} : [-1,1]^{d_X} \to \mathbb{R}^{d_H}$ modelling the jumps when new observations are made, and
- $g_{\theta_3} : \mathbb{R}^{d_H} \to \mathbb{R}^{d_Y}$ the readout map, mapping into the target space $\mathcal{Y} \subset \mathbb{R}^{d_Y}$ for $d_Y \in \mathbb{N}$.

The trainable parameters of the neural networks are $\theta := (\theta_1, \theta_2, \theta_3) \in \Theta := \cup_{M \geq 1} \Theta_M$. Here, for every $M \in \mathbb{N}$, Θ_M is defined to be the set of all parameters such that f_{θ_1} and ρ_{θ_2} have hidden dimension M. We define the pure jump stochastic process (cf. Appendix C)

$$u : \tilde{\Omega} \times [0,T] \to \mathbb{R}, (\tilde{\omega}, t) \mapsto u_t(\tilde{\omega}) := \sum_{i=1}^{n(\tilde{\omega})} \mathbf{1}_{[t_i(\tilde{\omega}), \infty)}(t).$$

Then the *neural jump ODE* (NJ-ODE) is defined by the latent process $H := (H_t)_{t \in [0,T]}$ and the output process $Y := (Y_t)_{t \in [0,T]}$ defined as solutions of the SDE system (cf. Appendix C)

$$\begin{aligned} H_0 &= \rho_{\theta_2}\left(\tanh(X_0)\right), \\ dH_t &= f_{\theta_1}\left(\tanh(H_{t-}), \tanh(X_{\tau(t)}), \tau(t), t - \tau(t)\right) dt + \left(\rho_{\theta_2}\left(\tanh(X_t)\right) - H_{t-}\right) du_t, \\ Y_t &= g_{\theta_3}(H_t). \end{aligned} \tag{30}$$

We apply the hyperbolic tangent function to each component of every input variable except for the time variables, before passing them to the network.[7] This ensures that every input to the neural networks is bounded in the compact sets where f_{θ_1} and ρ_{θ_2} are defined. Compactness of the domain is an assumption needed to apply the universal approximation theorem by Hornik et al. (1989).

Note that, only the values of X at the times $t_i, 0 \leq i \leq n$ are used as inputs. We will use the notation $H_t^\theta(X)$ and $Y_t^\theta(X)$ to emphasize the dependence of the latent process H and the output process Y on the model parameters θ and the input X.

Existence and uniqueness. We note that u is an adapted process starting at 0 with finite variation on the product probability space $(\Omega \times \tilde{\Omega}, \mathcal{F} \otimes \tilde{\mathcal{F}}, \mathbb{F} \otimes \tilde{\mathcal{F}}, \mathbb{P} \times \tilde{\mathbb{P}})$, since the total variation of u up to time T is n and $\mathbb{E}_{\mathbb{P} \times \tilde{\mathbb{P}}}[n] < \infty$. Hence, since f_{θ_1} and ρ_{θ_2} are Lipschitz continuous (as composition of Lipschitz continuous functions) a unique càdlàg solution H^θ exists, once an initial value is fixed (Protter, 2005, Thm. 7, Chap. V). Moreover, the resulting process $(Y_t^\theta)_{t \in [0,T]}$ is also càdlàg and $\mathbb{A}$-adapted.

Equivalent way of writing NJ-ODE. By applying the steps that were explained in Section C backwards to (30) (but without introducing the residual version of the RNN), it is easy to see that our model can equivalently be written (similar to (23)) as

$$\begin{cases} h_{t_{i+1}-} &:= \text{ODESolve}(f_{\theta_1}, (\tanh(h_t), \tanh(x_{t_i}), t_i, t - t_i), (t_i, t_{i+1})) \\ h_{t_{i+1}} &:= \rho_{\theta_2}(\tanh(x_{t_{i+1}})) \,. \end{cases} \tag{31}$$

In particular, the main difference to (23) is that we use a modified input for f_{θ_1} and that the neural network performing the jumps does not take $h_{t_{i+1}-}$ as an input, i.e. it is not a RNN.

[7] By abuse of notation we will write $\tanh(x)$ when applying the $\tanh$ element wise to a vector x.

D.2 OBJECTIVE FUNCTION

We introduce a loss function, such that the output Y^θ of the NJ-ODE can be trained to approximate $\hat{X}$, i.e. to model the best *on-line* prediction of the stochastic process X. We define the theoretical loss function and its Monte Carlo and Ergodic approximation.

Objective function. Let us define $\mathbb{D}$ to be the set of all $\mathbb{R}^{d_X}$-valued $\mathbb{A}$-adapted processes on the probability space $(\Omega \times \tilde{\Omega}, \mathcal{F} \otimes \tilde{\mathcal{F}}, \mathbb{F} \otimes \tilde{\mathcal{F}}, \mathbb{P} \times \tilde{\mathbb{P}})$. Then we define our objective functions

$$\Psi : \mathbb{D} \to \mathbb{R}, \qquad Z \mapsto \Psi(Z) := \mathbb{E}_{\mathbb{P}\times\tilde{\mathbb{P}}}\left[\frac{1}{n}\sum_{i=1}^{n}\left(|X_{t_i} - Z_{t_i}|_2 + |Z_{t_i} - Z_{t_i-}|_2\right)^2\right], \tag{32}$$

$$\Phi : \Theta \to \mathbb{R}, \qquad \theta \mapsto \Phi(\theta) := \Psi(Y^\theta(X)), \tag{33}$$

where Φ will be our (theoretical) loss function. Remark that from the definition of Y^θ, it directly follows that it is an element of $\mathbb{D}$, hence Φ is well-defined.

Monte Carlo approximation of the objective function. Let us assume, that we observe $N \in \mathbb{N}$ independent realisations of the path X at times $(\tilde{t}_1^j, \cdots, \tilde{t}_{n(j)}^j)$, $1 \le j \le N$, which are themselves independent realisations of the random vector $(n, t_1, \cdots, t_n)$. In particular, let us assume that $X^j \sim X$ and $(n^j, t_1^j, \cdots, t_{n^j}^j) \sim \mathbb{P}_t$ are i.i.d. random processes (respectively variables) for $1 \le j \le N$ and that our training data is one realisation of them. Then

$$\hat{\Phi}_N(\theta) := \frac{1}{N}\sum_{j=1}^{N}\frac{1}{n^j}\sum_{i=1}^{n^j}\left(\left|X^j_{t_i^j} - Y^\theta_{t_i^j}(X^j)\right|_2 + \left|Y^\theta_{t_i^j}(X^j) - Y^\theta_{t_i^j-}(X^j)\right|_2\right)^2, \tag{34}$$

converges $(\mathbb{P} \times \tilde{\mathbb{P}})$-a.s. to $\Phi(\theta)$ as $N \to \infty$, by the law of large numbers (cf. Theorem E.12). Therefore, (34) is a good approximation of Φ (33) that can be used in practice. However, our theoretical result makes use of the limiting loss function Φ, i.e. we assume to be in the case of having infinitely many independent training samples.

Ergodic approximation of the objective function. If we only observe one realization of the path X at times $(\tilde{t}_1, \cdots, \tilde{t}_N)$, we can still approximate the objective function by assuming that μ and σ are time-independent and that the stochastic process X is ergodic in the following sense. We fix $n = 1$ and assume that the time increments $\Delta\tilde{t}_j := \tilde{t}_j - \tilde{t}_{j-1}$ are i.i.d. realizations of the probability distribution λ_1. Furthermore, we consider each observation $X_{\tilde{t}_j}$ as one sample with initial condition $X_{\tilde{t}_{j-1}}$ for which $Y^{\theta,j}$ is the realization of Y^θ. Then we approximate the objective function by

$$\hat{\Phi}_N(\theta) := \frac{1}{N}\sum_{j=1}^{N}\left(\left|X_{\tilde{t}_j} - Y^\theta_{\Delta\tilde{t}_j}(X)\right|_2 + \left|Y^\theta_{\Delta\tilde{t}_j}(X) - Y^\theta_{\Delta\tilde{t}_j-}(X)\right|_2\right)^2, \tag{35}$$

which is assumed to converge by the ergodicity assumption for $N \to \infty$ to

$$\mathbb{E}_{\mathbb{P}\times\tilde{\mathbb{P}}}\left[\left(\left|X_{t_1} - Y^\theta_{t_1}\right|_2 + \left|Y^\theta_{t_1} - Y^\theta_{t_1-}\right|_2\right)^2\right]. \tag{36}$$

Instead of setting the random variable $n = 1$, one could similarly fix the time horizon T, and take for each sample all subsequent observations that lie in the time interval $[t_{\text{start}}, t_{\text{start}} + T]$, where t_{start} is the date of the first observation of this sample. The next sample would then start with the first observation after $t_{\text{start}} + T$.

E THEORETICAL CONVERGENCE RESULTS

Our main results show, that the output of NJ-ODE converges to the conditional expectation when the size of the neural networks and the number of samples go to infinity. For each network size (and number of samples) we assume to have the weights minimizing the (Monte Carlo approximation of the) loss function. In particular, we do not consider the problem of finding those optimal weights, and therefore also do not analyse backpropagation through our model. In a similar setting, backpropagation was studied by Jia & Benson (2019).

For completeness we recall the definition of L^p-convergence.

Definition E.1. *Let $1 \leq p < \infty$. Let $(\Omega, \mathcal{F}, \mathbb{P})$ be a probability space. Then a sequence of random variables $(X_n)_{n\in\mathbb{N}}$ converges to a random variable X in $L^p(\Omega, \mathcal{F}, \mathbb{P})$ (or simply L^p), if*

$$\mathbb{E}[|X_n - X|^p] \xrightarrow{n\to\infty} 0.$$

We use the notation

$$X_n \xrightarrow{L^p} X.$$

L^1-convergence is also denoted convergence in mean.

E.1 Convergence with respect to theoretical objective function

Theorem E.2. *Let $\theta_M^{\min} \in \Theta_M^{\min} := \operatorname{argmin}_{\theta\in\Theta_M}\{\Phi(\theta)\}$ for every $M \in \mathbb{N}$. Then, for $M \to \infty$, the value of the loss function Φ (33) converges to the minimal value of Ψ (32) which is uniquely achieved by $\hat{X}$, i.e.*

$$\Phi(\theta_M^{\min}) \xrightarrow{M\to\infty} \min_{Z\in\mathbb{D}} \Psi(Z) = \Psi(\hat{X}).$$

Furthermore, for every $1 \leq k \leq K$ we have that $Y^{\theta_M^{\min}}$ converges to $\hat{X}$ as random variable in $L^1(\Omega \times [0,T], \mathbb{P} \times \lambda_k)$. In particular, the limit process $Y := \lim_{M\to\infty} Y^{\theta_M^{\min}}$ equals $\hat{X}$ $(\mathbb{P} \times \lambda_k)$-almost surely as a random variable on $\Omega \times [0,T]$.

The idea of the proof is to split up the target jump process into its continuous-in-time parts and into the jumps. Both parts are continuous functions of their inputs and can therefore be approximated by neural networks (Hornik et al., 1989). More precisely, by Proposition B.1 and B.4 the continuous-in-time part can be written as an integral over time of a function which is jointly continuous in its inputs. This jointly continuous function is approximated by a neural network, which is itself integrated over time – that is the neural ODE part of the NJ-ODE. The remainder of the proof shows L^1-convergence of the output of NJ-ODE with optimal weights (with respect to the loss function) to the conditional expectation process.

For completeness we restate the straight forward generalization of the universal approximation result (Hornik et al., 1989, Thm. 2.4) to multidimensional output.

Theorem E.3 (Hornik)**.** *Let $r, d \in \mathbb{N}$ and σ be a sigmoid function. Let $\mathcal{NN}_{r,d}^{\sigma}$ be the set of all 1-hidden layer neural networks mapping $\mathbb{R}^r$ to $\mathbb{R}^d$. Then for every compact subset $K \subset \mathbb{R}^r$, every $\epsilon > 0$ and every $f \in C(\mathbb{R}^r, \mathbb{R}^d)$ there exists a neural network $g \in \mathcal{NN}_{r,d}^{\sigma}$ such that $\sup_{x\in K}|f(x) - g(x)|_2 < \epsilon$.*

The following Lemmas are used in the Proof of Theorem E.2.

Lemma E.4. *Let $1 \leq k \leq K$ and let $Z \in \mathbb{D}$ be a process such that $(\mathbb{P} \times \lambda_k)[\hat{X} \neq Z] > 0$. Then there exists an $\varepsilon > 0$ such that $\tilde{B} := \{t \in [0,T] \,|\, \mathbb{E}_{\mathbb{P}}[|X_t - Z_{t-}|_2^2] \geq \varepsilon + \mathbb{E}_{\mathbb{P}}[|X_t - \hat{X}_{t-}|_2^2]\}$ satisfies $\lambda_k(\tilde{B}) > 0$.*

Proof. First remark that since X is continuous, we have $X_t = X_{t-}$. Let us define $C := \{(\omega, t) \in \Omega \times [0,T] \,|\, \hat{X}_{t-}(\omega) \neq Z_{t-}(\omega)\}$ and for each $t \in [0,T]$ let $C_t := \{\omega \in \Omega \,|\, (\omega, t) \in C\}$. Then we have for $B := \{t \in [0,T] \,|\, \mathbb{P}(C_t) > 0\}$ that $\lambda_k(B) > 0$, since otherwise by Fubini's theorem

$$0 < (\mathbb{P} \times \lambda_k)[C] = \int_{[0,T]} \mathbb{P}(C_t) d\lambda_k(t) = 0,$$

which is a contradiction. Now Proposition B.2 yields that for each $t \in B$ there exists some $\varepsilon_t > 0$ such that $\mathbb{E}_{\mathbb{P}}[|X_{t-} - Z_{t-}|_2^2] \geq \varepsilon_t + \mathbb{E}_{\mathbb{P}}[|X_{t-} - \hat{X}_{t-}|_2^2]$. This implies the claim. Indeed, assume no such $\varepsilon > 0$ exists, then we have for each $n \in \mathbb{N}$ that $\lambda_k\left(\{t \in [0,T] \,|\, \mathbb{E}_{\mathbb{P}}[|X_{t-} - Z_{t-}|_2^2] \geq \frac{1}{n} + \mathbb{E}_{\mathbb{P}}[|X_{t-} - \hat{X}_{t-}|_2^2]\}\right) = 0$. Therefore,

$$\begin{aligned}
&\lambda_k\left(\{t \in [0,T] \,|\, \mathbb{E}_{\mathbb{P}}[|X_{t-} - Z_{t-}|_2^2] > \mathbb{E}_{\mathbb{P}}[|X_{t-} - \hat{X}_{t-}|_2^2]\}\right) \\
&\quad \leq \sum_{n\in\mathbb{N}} \lambda_k\left(\{t \in [0,T] \,|\, \mathbb{E}_{\mathbb{P}}[|X_{t-} - Z_{t-}|_2^2] \geq \tfrac{1}{n} + \mathbb{E}_{\mathbb{P}}[|X_{t-} - \hat{X}_{t-}|_2^2]\}\right) = 0,
\end{aligned}$$

which is a contradiction to $\lambda_k(B) > 0$. □

Lemma E.5. *For any $\mathbb{A}$-adapted process Z it holds that*

$$\mathbb{E}_{\mathbb{P}\times\tilde{\mathbb{P}}}\left[\frac{1}{n}\sum_{i=1}^{n}|X_{t_i}-Z_{t_i-}|_2^2\right]=\mathbb{E}_{\mathbb{P}\times\tilde{\mathbb{P}}}\left[\frac{1}{n}\sum_{i=1}^{n}\left|X_{t_i}-\hat{X}_{t_i-}\right|_2^2\right]+\mathbb{E}_{\mathbb{P}\times\tilde{\mathbb{P}}}\left[\frac{1}{n}\sum_{i=1}^{n}\left|\hat{X}_{t_i-}-Z_{t_i-}\right|_2^2\right].$$

Proof. First recall that by continuity $X_{t_i}=X_{t_i-}$. Then the statement is a consequence of Proposition B.2, Lemma B.3 and Fubini's theorem, which imply

$$\begin{aligned}\mathbb{E}_{\mathbb{P}\times\tilde{\mathbb{P}}}\left[\frac{1}{n}\sum_{i=1}^{n}|X_{t_i-}-Z_{t_i-}|_2^2\right]&=\mathbb{E}_{\tilde{\mathbb{P}}}\left[\frac{1}{n}\sum_{i=1}^{n}\mathbb{E}_{\mathbb{P}}\left[|X_{t_i-}-Z_{t_i-}|_2^2\right]\right]\\&=\mathbb{E}_{\tilde{\mathbb{P}}}\left[\frac{1}{n}\sum_{i=1}^{n}\left(\mathbb{E}_{\mathbb{P}}\left[\left|X_{t_i-}-\hat{X}_{t_i-}\right|_2^2\right]+\mathbb{E}_{\mathbb{P}}\left[\left|\hat{X}_{t_i-}-Z_{t_i-}\right|_2^2\right]\right)\right]\\&=\mathbb{E}_{\mathbb{P}\times\tilde{\mathbb{P}}}\left[\frac{1}{n}\sum_{i=1}^{n}\left|X_{t_i-}-\hat{X}_{t_i-}\right|_2^2\right]+\mathbb{E}_{\mathbb{P}\times\tilde{\mathbb{P}}}\left[\frac{1}{n}\sum_{i=1}^{n}\left|\hat{X}_{t_i-}-Z_{t_i-}\right|_2^2\right].\end{aligned}$$

□

Lemma E.6. *Let $1\leq p<\infty$. Let $(Z_n)_{n\in\mathbb{N}}$ be a sequence of random variables, and Z and $\tilde{Z}$ random variables defined on a common probability space such that $Z_n\xrightarrow{L^p}Z$ and $Z_n\xrightarrow{L^p}\tilde{Z}$. Then $Z=\tilde{Z}$ almost surely.*

Proof. With the triangle inequality it follows that $\mathbb{E}[|Z-\tilde{Z}|^p]^{1/p}=0$, which implies the claim. □

Proof of Theorem E.2. We start by showing that $\hat{X}\in\mathbb{D}$ is the unique minimizer of Ψ up to $(\mathbb{P}\times\lambda_k)$-null-sets for any $k\leq K$. First, we recall that for every t_i we have $\hat{X}_{t_i}=X_{t_i}$ and by continuity of X that $X_{t_i}=X_{t_i-}$. Therefore,

$$\begin{aligned}\Psi(\hat{X})&=\mathbb{E}_{\mathbb{P}\times\tilde{\mathbb{P}}}\left[\frac{1}{n}\sum_{i=1}^{n}\left|X_{t_i}-\hat{X}_{t_i-}\right|_2^2\right]\\&=\mathbb{E}_{\tilde{\mathbb{P}}}\left[\frac{1}{n}\sum_{i=1}^{n}\mathbb{E}_{\mathbb{P}}\left[\left|X_{t_i}-\hat{X}_{t_i-}\right|_2^2\right]\right]\\&=\min_{Z\in\mathbb{D}}\mathbb{E}_{\mathbb{P}\times\tilde{\mathbb{P}}}\left[\frac{1}{n}\sum_{i=1}^{n}|X_{t_i}-Z_{t_i-}|_2^2\right]\\&\leq\min_{Z\in\mathbb{D}}\mathbb{E}_{\mathbb{P}\times\tilde{\mathbb{P}}}\left[\frac{1}{n}\sum_{i=1}^{n}\left(|X_{t_i}-Z_{t_i}|_2+|Z_{t_i}-Z_{t_i-}|_2\right)^2\right]\\&=\min_{Z\in\mathbb{D}}\Psi(Z),\end{aligned}$$

where we used Fubini's theorem for the second line, Proposition B.2 for the third line and the triangle inequality for the fourth line. Hence, $\hat{X}$ is a minimizer of Ψ. To see that it is unique $(\mathbb{P}\times\lambda_k)$-a.s., let $Z\in\mathbb{D}$ be a process such that $(\mathbb{P}\times\lambda_k)[\hat{X}\neq Z]>0$. By Lemma E.4, this implies that there exists an $\varepsilon>0$ such that $B:=\{t\in[0,T]\,|\,\mathbb{E}_{\mathbb{P}}[|X_{t-}-Z_{t-}|_2^2]\geq\epsilon+\mathbb{E}_{\mathbb{P}}[|X_{t-}-\hat{X}_{t-}|_2^2]\}$ satisfies $\lambda_k(B)>0$.

Now recall that by definition of λ_k we have $\lambda_k(B)=\tilde{\mathbb{P}}(\dot{\cup}_{j\geq k}\{n=j,t_k-\in B\})/\tilde{\mathbb{P}}(n\geq k)>0$. This implies that there exists $j\in\mathbb{N}_{\geq k}$ such that $\tilde{\mathbb{P}}(n=j,t_k-\in B)>0$. Therefore,

$$\begin{aligned}\mathbb{E}_{\tilde{\mathbb{P}}}\left[\frac{1}{n}\sum_{i=1}^{n}\mathbf{1}_{\{t_i-\in B\}}\right]&\geq\mathbb{E}_{\tilde{\mathbb{P}}}\left[\mathbf{1}_{\{n=j\}}\frac{1}{n}\sum_{i=1}^{n}\mathbf{1}_{\{t_i-\in B\}}\right]\\&\geq\mathbb{E}_{\tilde{\mathbb{P}}}\left[\mathbf{1}_{\{n=j\}}\tfrac{1}{j}\mathbf{1}_{\{t_k-\in B\}}\right]\\&=\tfrac{1}{j}\tilde{\mathbb{P}}(n=j,t_k-\in B)>0.\end{aligned}$$

This inequality implies now that Z is not a minimizer of Ψ, because

$$\begin{aligned}
\Psi(Z) &= \mathbb{E}_{\mathbb{P}\times\tilde{\mathbb{P}}}\left[\frac{1}{n}\sum_{i=1}^{n}\left(|X_{t_i}-Z_{t_i}|_2+|Z_{t_i}-Z_{t_i-}|_2\right)^2\right] \\
&\geq \mathbb{E}_{\tilde{\mathbb{P}}}\left[\frac{1}{n}\sum_{i=1}^{n}\mathbb{E}_{\mathbb{P}}\left[|X_{t_i}-Z_{t_i-}|_2^2\right]\right] \\
&= \mathbb{E}_{\tilde{\mathbb{P}}}\left[\frac{1}{n}\sum_{i=1}^{n}\left(\mathbf{1}_{\{t_i-\in B\}}+\mathbf{1}_{\{t_i-\in B^C\}}\right)\mathbb{E}_{\mathbb{P}}\left[|X_{t_i}-Z_{t_i-}|_2^2\right]\right] \\
&\geq \mathbb{E}_{\tilde{\mathbb{P}}}\left[\frac{1}{n}\sum_{i=1}^{n}\left(\varepsilon\,\mathbf{1}_{\{t_i-\in B\}}+\mathbb{E}_{\mathbb{P}}\left[\left|X_{t_i}-\hat{X}_{t_i-}\right|_2^2\right]\right)\right] \\
&= \varepsilon\,\mathbb{E}_{\tilde{\mathbb{P}}}\left[\frac{1}{n}\sum_{i=1}^{n}\mathbf{1}_{\{t_i-\in B\}}\right]+\min_{Z\in\mathbb{D}}\Psi(Z) \\
&> \min_{Z\in\mathbb{D}}\Psi(Z).
\end{aligned}$$

Next we show that (30) can approximate $\hat{X}$ arbitrarily well. Since the dimension d_H can be chosen freely, let us fix it to $d_H := d_X$. Furthermore, let us fix θ_3^* such that $g_{\theta_3^*} = \mathrm{id}$. From Theorem E.3 it follows that for any $\varepsilon > 0$ there exist $M \in \mathbb{N}$ and θ_1^*, θ_2^* with $(\theta_1^*, \theta_2^*, \theta_3^*) \in \Theta_M$ such that

$$\sup_{\tilde{u}\in d_X}\left|\rho_{\theta_2^*}\left(\tanh(\tilde{u})\right)-\tilde{u}\right|_2 = \sup_{u\in[-1,1]^{d_X}}\left|\rho_{\theta_2^*}\left(u\right)-\tanh^{-1}(u)\right)|_2 \leq \varepsilon, \tag{37}$$

and

$$\begin{aligned}
&\sup_{(\tilde{u},\tilde{v},t,r)\in\mathbb{R}^{d_H\times d_X}\times\Delta}\left|f_{\theta_1^*}\left(\tanh(\tilde{u}),\tanh(\tilde{v}),t,r\right)-\tilde{\mu}\left(\tilde{v},t,r\right)\right|_2 \\
&\qquad = \sup_{(u,v,t,r)\in[-1,1]^{d_H\times d_X}\times\Delta}\left|f_{\theta_1^*}\left(u,v,t,r\right)-\tilde{\mu}\left(\tanh^{-1}(v),t,r\right)\right|_2 \leq \varepsilon,
\end{aligned} \tag{38}$$

where we used that $\tilde{\mu}$ is continuous by Proposition B.4 and substituted $u = \tanh(\tilde{u}), v = \tanh(\tilde{v})$. Using this, we can bound the distance between $Y_t^{\theta_M^*}$ and $\hat{X}$. In particular, if $t \in \{t_1, \cdots, t_n\}$, (37) yields

$$\left|Y_t^{\theta_M^*}-\hat{X}_t\right|_2 = \left|\left(H_{t-}+\left(\rho_{\theta_M^*}(\tanh(X_t))-H_{t-}\right)\right)-X_t\right|_2 \leq \varepsilon,$$

and if t not in $\{t_1, \cdots, t_n\}$, then (13), (38) and the previous bound yield

$$\begin{aligned}
\left|Y_t^{\theta_M^*}-\hat{X}_t\right|_2 &\leq \left|Y_{\tau(t)}^{\theta_M^*}-\hat{X}_{\tau(t)}\right|_2 \\
&\quad+\int_{\tau(t)}^{t}\left|f_{\theta_1^*}\left(\tanh(H_{s-}),\tanh(X_{\tau(s)}),\tau(s),s-\tau(s)\right)-\tilde{\mu}\left(X_{\tau(s)},\tau(s),s-\tau(s)\right)\right|_2 ds \\
&\leq \varepsilon+\varepsilon T.
\end{aligned}$$

Now we can show the convergence of $\Phi(\theta_M^{\min})$ using these two bounds and $X_{t_i} = \hat{X}_{t_i}$. Indeed,

$$\begin{aligned}
\min_{Z\in\mathbb{D}} \Psi(Z) &\leq \Phi(\theta_M^{\min}) \leq \Phi(\theta_M^*) \\
&= \mathbb{E}_{\mathbb{P}\times\tilde{\mathbb{P}}}\left[\frac{1}{n}\sum_{i=1}^n \left(\left|X_{t_i} - Y_{t_i}^{\theta_M^*}\right|_2 + \left|Y_{t_i}^{\theta_M^*} - Y_{t_i-}^{\theta_M^*}\right|_2\right)^2\right] \\
&\leq \mathbb{E}_{\mathbb{P}\times\tilde{\mathbb{P}}}\left[\frac{1}{n}\sum_{i=1}^n \left(\left|\hat{X}_{t_i} - Y_{t_i}^{\theta_M^*}\right|_2 + \left|Y_{t_i}^{\theta_M^*} - \hat{X}_{t_i}\right|_2 + \left|\hat{X}_{t_i} - \hat{X}_{t_i-}\right|_2 + \left|\hat{X}_{t_i-} - Y_{t_i-}^{\theta_M^*}\right|_2\right)^2\right] \\
&\leq \mathbb{E}_{\mathbb{P}\times\tilde{\mathbb{P}}}\left[\frac{1}{n}\sum_{i=1}^n \left(\varepsilon + \varepsilon + \left|X_{t_i} - \hat{X}_{t_i-}\right|_2 + \varepsilon\,(T+1)\right)^2\right] \\
&\leq \varepsilon^2\,(T+3)^2 + \mathbb{E}_{\mathbb{P}\times\tilde{\mathbb{P}}}\left[\frac{1}{n}\sum_{i=1}^n \left(2\varepsilon\,(T+3)\left|X_{t_i} - \hat{X}_{t_i-}\right|_2 + \left|X_{t_i} - \hat{X}_{t_i-}\right|_2^2\right)\right] \\
&\leq \varepsilon^2\,(T+3)^2 + 2\varepsilon\,(T+3)\,\mathbb{E}_{\mathbb{P}\times\tilde{\mathbb{P}}}\left[\frac{1}{n}\sum_{i=1}^n \left|X_{t_i} - \hat{X}_{t_i-}\right|_2\right] + \mathbb{E}_{\mathbb{P}\times\tilde{\mathbb{P}}}\left[\frac{1}{n}\sum_{i=1}^n \left|X_{t_i} - \hat{X}_{t_i-}\right|_2^2\right] \\
&\leq \varepsilon^2\,(T+3)^2 + 2\varepsilon\,(T+3)\left(\min_{Z\in\mathbb{D}}\Psi(Z) + 1\right) + \min_{Z\in\mathbb{D}}\Psi(Z) \xrightarrow{\varepsilon\to 0} \min_{Z\in\mathbb{D}}\Psi(Z),
\end{aligned}$$

where we used $\Psi(\hat{X}) = \min_{Z\in\mathbb{D}}\Psi(Z)$ and that for $a \in \mathbb{R}$, $a \leq a^2 + 1$ in the last step. It is clear from the construction before, that $\varepsilon \to 0$ as $M \to \infty$.

In the last step we show that the limits $\lim_{M\to\infty} Y^{\theta_M^{\min}}$ and $\lim_{M\to\infty} Y^{\theta_M^*}$ exist as limits in the Banach space $\mathbb{L} := L^1(\Omega \times [0,T], \mathbb{F}\otimes\mathcal{B}([0,T]), \mathbb{P}\times\lambda_k)$, for every $k \leq K$, and that they are both equal to $\hat{X}$. Let us fix $k \leq K$. First we note that for every $B \in \mathcal{B}([0,T])$ we have

$$\mathbb{E}_{\lambda_k}[\mathbf{1}_B] = \lambda_k(B) = \frac{\tilde{\mathbb{P}}(n\geq k, t_k - \in B)}{\tilde{\mathbb{P}}(n\geq k)} = \frac{\mathbb{E}_{\tilde{\mathbb{P}}}[\mathbf{1}_{\{n\geq k\}}\mathbf{1}_{\{t_k-\in B\}}]}{\tilde{\mathbb{P}}(n\geq k)}.$$

Using "measure theoretic induction" (Durrett, 2010, Case 1-4 of Proof of Thm. 1.6.9) this yields for $c := (\mathbb{P}(n\geq k))^{-1}$ and a $\mathcal{B}([0,T])$-measurable function $Z : [0,T] \to \mathbb{R}, t \mapsto Z_t := Z(t)$ that

$$\mathbb{E}_{\lambda_k}[Z] = c\,\mathbb{E}_{\tilde{\mathbb{P}}}[\mathbf{1}_{\{n\geq k\}} Z_{t_k-}]. \tag{39}$$

Moreover, the triangle inequality and Lemma E.5 yield

$$\begin{aligned}
\Phi(\theta_M^*) - \Psi(\hat{X}) &\geq \mathbb{E}_{\mathbb{P}\times\tilde{\mathbb{P}}}\left[\tfrac{1}{n}\sum_{i=1}^n \left|X_{t_i} - Y_{t_i-}^{\theta_M^*}\right|_2^2\right] - \Psi(\hat{X}) \\
&= \mathbb{E}_{\mathbb{P}\times\tilde{\mathbb{P}}}\left[\tfrac{1}{n}\sum_{i=1}^n \left|\hat{X}_{t_i-} - Y_{t_i-}^{\theta_M^*}\right|_2^2\right].
\end{aligned} \tag{40}$$

For any $\mathbb{R}^{d_X}$-valued $Z \in \mathbb{L}$ the Hölder inequality, together with the fact that $n \geq 1$, yields

$$\mathbb{E}_{\mathbb{P}\times\tilde{\mathbb{P}}}\left[|Z|_2\right] = \mathbb{E}_{\mathbb{P}\times\tilde{\mathbb{P}}}\left[\frac{\sqrt{n}}{\sqrt{n}}|Z|_2\right] \leq \mathbb{E}_{\mathbb{P}\times\tilde{\mathbb{P}}}[n]^{1/2}\,\mathbb{E}_{\mathbb{P}\times\tilde{\mathbb{P}}}\left[\frac{1}{n}|Z|_2^2\right]^{1/2}. \tag{41}$$

Together, this implies that $\lim_{M\to\infty} Y^{\theta_M^*} = \hat{X}$ as a $\mathbb{L}$-limit. Indeed, with $\tilde{c} := \mathbb{E}_{\mathbb{P}\times\tilde{\mathbb{P}}}[n]^{1/2} < \infty$ we have

$$\begin{aligned}
\mathbb{E}_{\mathbb{P}\times\lambda_k}\left[\left|\hat{X} - Y^{\theta_M^*}\right|_2\right] &= c\,\mathbb{E}_{\mathbb{P}\times\tilde{\mathbb{P}}}\left[\mathbf{1}_{\{n\geq k\}}\left|\hat{X}_{t_k-} - Y^{\theta_M^*}_{t_k-}\right|_2\right] \\
&\leq c\,\tilde{c}\,\mathbb{E}_{\mathbb{P}\times\tilde{\mathbb{P}}}\left[\mathbf{1}_{\{n\geq k\}}\frac{1}{n}\left|\hat{X}_{t_k-} - Y^{\theta_M^*}_{t_k-}\right|_2^2\right]^{1/2} \\
&\leq c\,\tilde{c}\,\mathbb{E}_{\mathbb{P}\times\tilde{\mathbb{P}}}\left[\mathbf{1}_{\{n\geq k\}}\frac{1}{n}\sum_{i=1}^{n}\left|\hat{X}_{t_i-} - Y^{\theta_M^*}_{t_i-}\right|_2^2\right]^{1/2} \\
&\leq c\,\tilde{c}\,\mathbb{E}_{\mathbb{P}\times\tilde{\mathbb{P}}}\left[\frac{1}{n}\sum_{i=1}^{n}\left|\hat{X}_{t_i-} - Y^{\theta_M^*}_{t_i-}\right|_2^2\right]^{1/2} \\
&\leq c\,\tilde{c}\left(\Phi(\theta_M^*) - \Psi(\hat{X})\right)^{1/2} \xrightarrow{M\to\infty} 0,
\end{aligned}$$

where we used first (39) and (41) followed by two simply upper bounds and (40) in the last step. The same argument can be applied to show that $\lim_{M\to\infty} Y^{\theta_M^{\min}} = \hat{X}$ as a $\mathbb{L}$-limit. In particular, this proves that the limit $Y := \lim_{M\to\infty} Y^{\theta_M^{\min}}$ exists as $\mathbb{L}$-limit and by Lemma E.6 it equals $\hat{X}$ $(\mathbb{P}\times\lambda_k)$-almost surely, for any $k \leq K$. □

Remark E.7. *This result can be extended to any other neural network architecture for which a universal approximation theorem equivalent to (Hornik et al., 1989, Thm. 2.4) exists. Moreover, the stochastic process X defined in (10) can be chosen more general, in particular, the diffusion part $\int \sigma dW$ can be replaced by any martingale, as long as the resulting process still is a Markov process and $\tilde{\mu}$ stays continuous.*

Remark E.8. *If we used the modified loss function $\tilde{\Psi}$ which is identical to Ψ except that we drop the factor $\frac{1}{n}$, everything would work similarly and we could show L^2-convergence instead of L^1-convergence of $Y^{\theta_M^{\min}}$ to $\hat{X}$. However, we remark that there might exists $Z \in \mathbb{D}$, such that $\Psi(Z) < \infty$ while $\tilde{\Psi}(Z) = \infty$. In particular, if some moment of n does not exist, such a process can be constructed.*

Remark E.9. *It follows directly from Theorem E.2 that $\lim_{M\to\infty} Y^{\theta_M^{\min}} = \hat{X}$ as random variables on $\Omega\times[0,T]$ except on sets which are null sets with respect to every product measure $\mathbb{P}\times\lambda_k$ for $1 \leq k \leq K$.*

Remark E.10. *The result of Theorem E.2 does not imply that $\hat{X}$ and $\lim_{M\to\infty} Y^{\theta_M^{\min}}$ are modifications or indistinguishable. For example, if $B \subset [0,T]$ is a subset such that no left-point of the observation times (t_k-) lies in B with probability greater 0, i.e. $\lambda_k(B) = 0$ for $1 \leq k \leq K$, then Theorem E.2 does not tell us how close $(\lim_{M\to\infty} Y^{\theta_M^{\min}})_t$ is to $\hat{X}_t$ for $t \in B$. In particular, it does not tell us whether they are equal $\mathbb{P}$-almost surely. Furthermore, such a set B always exists, since there has to exists $t \in [0,T]$ such that $B := \{t\}$ has measure 0 for all k.*

In the following corollary we show, that Theorem E.2 can be extended to show convergence to the conditional expectation of $\varphi(X)$, for some function $\varphi \in C^{2,b}(\mathbb{R}^{d_X},\mathbb{R})$, i.e. a function that is twice continuously differentiable with bounded derivatives.

Corollary E.11. *Let $\varphi \in C^{2,b}(\mathbb{R}^{d_X},\mathbb{R})$, then the statement of Theorem E.2 holds equivalently, when replacing X in the loss functions Ψ and Φ by $\Gamma = \varphi(X)$ and $\hat{X}$ by the conditional expectation $\hat{\Gamma}$, where $\hat{\Gamma}_t := \mathbb{E}_{\mathbb{P}\times\tilde{\mathbb{P}}}[\varphi(X_t)|\mathcal{A}_t]$.*

Corollary E.11 combined with the monotone convergence theorem for conditional expectation theoretically enables us to make statements about the conditional law and conditional moments of X under some a priori integrability assumptions.

Proof of Corollary E.11. We first remark that Proposition B.2 and Lemma E.4, E.5, B.3 hold similarly for the conditional expectation $\hat{\Gamma}$. Hence, the same argument as in the proof of Theorem E.2 implies that $\hat{\Gamma}$ is the unique $\mathbb{A}$-adapted minimizer of Ψ.
For simplicity of the notation we assume that $d_X = d_Y = 1$, i.e. that the process X and the Brownian

motion W are 1-dimensional. However, the following works as well in the general case, where the correlations of the Brownian motion components have to be taken into account. By Itô's Formula (Protter, 2005, Chap. II, Thm. 32), $\Gamma = \varphi(X)$ is the solution of the SDE

$$\begin{aligned} d\varphi(X)_t &= \varphi'(X_t)dX_t + \tfrac{1}{2}\varphi''(X_t)d[X,X]_t \\ &= \varphi'(X_t)\mu(t,X_t)dt + \varphi'(X_t)\sigma(t,X_t)dW_t + \tfrac{1}{2}\varphi''(X_t)\sigma(t,X_t)^2dt \\ &= \alpha(t,X_t)dt + \beta(t,X_t)dW_t, \end{aligned}$$

for $\alpha(t,X_t) := \varphi'(X_t)\mu(t,X_t) + \frac{1}{2}\varphi''(X_t)\sigma(t,X_t)^2$ and $\beta(t,X_t) := \varphi'(X_t)\sigma(t,X_t)$. Defining $\tilde{\alpha}$ similar to $\tilde{\mu}$ as

$$\tilde{\alpha} : \Delta \times \mathbb{R}^{d_X} \to \mathbb{R}^{d_X}, \quad (t,r,\xi) \mapsto P_{t,t+r}(X_t,\alpha)\big|_{X_t=\xi} = \mathbb{E}_{\mathbb{P}}\left[\alpha(t+r,X_{t+r})|X_t=\xi\right],$$

one can use the boundedness of of φ' and φ'' to show that it is continuous and that

$$\hat{\Gamma}_t = \mathbb{E}[\varphi(X)_t|\mathcal{A}_t] = \Gamma_{\tau(t)} + \int_{\tau(t)}^{t} \tilde{\alpha}\left(\tau(t), s-\tau(t), X_{\tau(t)}\right) ds.$$

In particular, Proposition B.1 and B.4 hold equivalently for Γ.
Similar to (37) and (38), the neural network parameters can be chosen such that

$$\sup_{\tilde{u}\in\mathbb{R}^{d_X}} \left|\rho_{\theta_2^*}(\tanh(\tilde{u})) - \varphi(\tilde{u})\right|_2 = \sup_{u\in[-1,1]^{d_X}} \left|\rho_{\theta_2^*}(u) - \varphi(\tanh^{-1}(u))\right|_2 \leq \varepsilon, \tag{42}$$

and

$$\begin{aligned} &\sup_{(\tilde{u},\tilde{v},t,r)\in\mathbb{R}^{d_H\times d_X}\times\Delta} \left|f_{\theta_1^*}(\tanh(\tilde{u}),\tanh(\tilde{v}),t,r) - \tilde{\alpha}(\tilde{v},t,r)\right|_2 \\ &\qquad = \sup_{(u,v,t,r)\in[-1,1]^{d_H\times d_X}\times\Delta} \left|f_{\theta_1^*}(u,v,t,r) - \tilde{\alpha}\left(\tanh^{-1}(v),t,r\right)\right|_2 \leq \varepsilon, \end{aligned} \tag{43}$$

which then implies the statement of the Corollary similar as in the proof of Theorem E.2. □

E.2 Convergence of the Monte Carlo approximation

In the following, we assume the size of the neural network M is fixed and we study the convergence with respect to the number of samples N. Moreover, we show that both types of convergence can be combined. To do so, we define $\tilde{\Theta}_M := \{\theta \in \Theta_M \mid |\theta|_2 \leq M\}$, which is a compact subspace of Θ_M. It is straight forward to see, that Θ_M in Theorem E.2 can be replaced by $\tilde{\Theta}_M$. Indeed, if the needed neural network weights for an ε-approximation have too large norm, then one can increase M until it is sufficiently big. Furthermore, we make the additional assumption that $\mathbb{E}_{\tilde{\mathbb{P}}}[n^2] < \infty$. The following convergence analysis is based on (Lapeyre & Lelong, 2019, Chapter 4.3).

Theorem E.12. *Let $\theta_{M,N}^{\min} \in \Theta_{M,N}^{\min} := \arg\inf_{\theta\in\tilde{\Theta}_M}\{\hat{\Phi}_N(\theta)\}$ for every $M,N\in\mathbb{N}$. Then, for every $M\in\mathbb{N}$, $(\mathbb{P}\times\tilde{\mathbb{P}})$-a.s.*

$$\hat{\Phi}_N \xrightarrow{N\to\infty} \Phi \quad \textit{uniformly on } \tilde{\Theta}_M.$$

Moreover, for every $M\in\mathbb{N}$, $(\mathbb{P}\times\tilde{\mathbb{P}})$-a.s.

$$\Phi(\theta_{M,N}^{\min}) \xrightarrow{N\to\infty} \Phi(\theta_M^{\min}) \quad \textit{and} \quad \hat{\Phi}_N(\theta_{M,N}^{\min}) \xrightarrow{N\to\infty} \Phi(\theta_M^{\min}).$$

In particular, one can define an increasing sequence $(N_M)_{M\in\mathbb{N}}$ in $\mathbb{N}$ such that for every $1\leq k\leq K$ we have that $Y^{\theta_{M,N_M}^{\min}}$ converges to $\hat{X}$ for $M\to\infty$ as random variable in $L^1(\Omega\times[0,T],\mathbb{P}\times\lambda_k)$. In particular, the limit process $Y := \lim_{M\to\infty} Y^{\theta_{M,N_M}^{\min}}$ equals $\hat{X}$ $(\mathbb{P}\times\lambda_k)$-almost surely as a random variable on $\Omega\times[0,T]$.

The following Monte Carlo convergence analysis is based on (Lapeyre & Lelong, 2019, Section 4.3). In comparison to them, we do not need the additional assumptions that were essential in (Lapeyre & Lelong, 2019, Section 4.3), i.e. that all minimizing neural network weights generate the same neural network output. This assumption is not needed, because we do not aim to show that $Y^{\theta_{M,N}^{\min}}$ converges to $Y^{\theta_M^{\min}}$.

We define the separable Banach space $\mathcal{S} := \{x = (x_i)_{\in\mathbb{N}} \in \ell^1(\mathbb{R}^{d_X}) \mid \exists n\in\mathbb{N} \text{ s.t. } \forall i>n : x_i = 0\}$ with the norm $\|x\|_{\ell^1} := \sum_{i\in\mathbb{N}}|x_i|_2$.

E.2.1 CONVERGENCE OF OPTIMIZATION PROBLEMS

Consider a sequence of real valued function $(f_n)_n$ defined on a compact set $K \subset \mathbb{R}^d$. Define, $v_n = \inf_{x \in K} f_n(x)$ and let x_n be a sequence of minimizers $f_n(x_n) = \inf_{x \in K} f_n(x)$.

From (Rubinstein & Shapiro, 1993, Theorem A1 and discussion thereafter) we have the following Lemma.

Lemma E.13. *Assume that the sequence $(f_n)_n$ converges uniformly on K to a continuous function f. Let $v^* = \inf_{x \in K} f(x)$ and $\mathcal{S}^* = \{x \in K : f(x) = v^*\}$. Then $v_n \to v^*$ and $d(x_n, \mathcal{S}^*) \to 0$ a.s.*

The following lemma is a consequence of (Ledoux & Talagrand, 1991, Corollary 7.10) and (Rubinstein & Shapiro, 1993, Lemma A1).

Lemma E.14. *Let $(\xi_i)_{i \geq 1}$ be a sequence of $i.i.d$ random variables with values in $\mathcal{S}$ and $h : \mathbb{R}^d \times \mathcal{S} \to \mathbb{R}$ be a measurable function. Here ℓ^1 denotes the space of sequences with absolutely convergent series. Assume that a.s, the function $\theta \in \mathbb{R} \mapsto h(\theta, \xi_1)$ is continuous and for all $C > 0$, $\mathbb{E}(\sup_{|\theta|_2 \leq C} |h(\theta, \xi_1)|) < +\infty$. Then, a.s $\theta \in \mathbb{R}^d \mapsto \frac{1}{N} \sum_{i=1}^N h(\theta, \xi_i)$ converges locally uniformly to the continuous function $\theta \in \mathbb{R}^d \mapsto \mathbb{E}(h(\theta, \xi_1))$.*

$$\lim_{N \to \infty} \sup_{|\theta|_2 \leq C} \left| \frac{1}{N} \sum_{i=1}^N h(\theta, \xi_i) - \mathbb{E}(h(\theta, \xi_1)) \right| = 0 \qquad a.s.$$

E.2.2 STRONG LAW OF LARGE NUMBERS

Let us define

$$F(\theta, x, y, z) := |x - y|_2 + |y - z|_2$$

and $\xi_j := (X^j_{t^j_1}, \dots, X^j_{t^j_{n^j}}, 0, \dots)$, where $X^j_{t^j_i}$ are random variables describing the realizations of the training data, as defined in Section D.2. By this definition we have $n^j := n^j(\xi_j) := \max_{i \in \mathbb{N}}\{\xi_{j,i} \neq 0\}$ $\mathbb{P}$-almost-surely and we know that ξ_j are i.i.d. random variables taking values in $\mathcal{S}$. Furthermore, let us write $Y^\theta_t(\xi)$ to make the dependence of Y on the input explicit. Then we define

$$h(\theta, \xi_j) := \frac{1}{n^j} \sum_{i=1}^{n^j} F\left(\theta, X_{t^j_i}, Y_{t^j_i}(\xi_j), Y_{t^j_i -}(\xi_j)\right)^2.$$

Lemma E.15. *The following properties are satisfied.*

- $(\mathcal{P}_1)$ *There exists $\kappa > 0$ such that for all $S \in \mathcal{S}$ and $\theta \in \tilde{\Theta}_M$ we have $|Y^\theta_t(S)|_2 \leq \kappa\, n(S)$ for all $t \in [0, T]$, where $n(S) = \max_{i \in \mathbb{N}}\{S_i \neq 0\}$.*
- $(\mathcal{P}_2)$ *Almost-surely the random function $\theta \in \tilde{\Theta}_M \mapsto Y^\theta_t$ is uniformly continuous for every $t \in [0, T]$.*
- $(\mathcal{P}_3)$ *We have $\mathbb{E}_{\mathbb{P} \times \tilde{\mathbb{P}}}\left[\frac{1}{n} \sum_{i=1}^n |X_{t_i}|_2^2\right] < \infty$ and $\mathbb{E}_{\mathbb{P} \times \tilde{\mathbb{P}}}\left[\frac{1}{n} \sum_{i=1}^n |X_{t_i -}|_2^2\right] < \infty$.*

Proof. By definition of the neural networks with sigmoid activation functions (in particular having bounded outputs), all neural network outputs are bounded in terms of the norm of the network weights, which is assumed to be bounded, not depending on the norm of the input. Since Y jumps at most $n(S)$ times, we can find κ depending on T, such that the claimed bound is satisfied for all t, proving $(\mathcal{P}_1)$.

Since the activation functions are continuous, also the neural networks are continuous with respect to their weights θ, which implies that also $\theta \in \tilde{\Theta}_M \mapsto Y^\theta_t$ is continuous. Since $\tilde{\Theta}_M$ is compact, this automatically yields uniform continuity and therefore finishes the proof of $(\mathcal{P}_2)$.

From our assumption that X is square integrable on the closed interval $[0, T]$, it follows that $\max_{0 \leq t \leq T} \mathbb{E}_{\mathbb{P}}[|X_t|^2] < \infty$. Hence, by independence we have

$$\mathbb{E}_{\mathbb{P} \times \tilde{\mathbb{P}}}\left[\frac{1}{n} \sum_{i=1}^n |X_{t_i}|_2^2\right] = \mathbb{E}_{\tilde{\mathbb{P}}}\left[\frac{1}{n} \sum_{i=1}^n \mathbb{E}_{\mathbb{P}}[|X_{t_i}|_2^2]\right] \leq \mathbb{E}_{\tilde{\mathbb{P}}}\left[\frac{1}{n} \sum_{i=1}^n \max_{0 \leq t \leq T} \mathbb{E}_{\mathbb{P}}[|X_t|_2^2]\right] = \max_{0 \leq t \leq T} \mathbb{E}_{\mathbb{P}}[|X_t|_2^2] < \infty,$$

and the same arguments shows $\mathbb{E}_{\mathbb{P} \times \tilde{\mathbb{P}}}\left[\frac{1}{n} \sum_{i=1}^n |X_{t_i -}|_2^2\right] < \infty$, therefore also $(\mathcal{P}_2)$ is proven. $\square$

Proof of Theorem E.12. We apply Lemma E.14 to the sequence of $i.i.d$ random function $h(\theta, \xi_j)$. From $(\mathcal{P}_1)$ of Lemma E.15 we have that

$$\begin{aligned} F(\theta, X_{t_i^j}, Y_{t_i^j}, Y_{t_i^j-})^2 &= \left(\left|X_{t_i^j} - Y^\theta_{t_i^j}\right|_2 + \left|Y^\theta_{t_i^j} - Y^\theta_{t_i^j-}\right|_2\right)^2 \\ &\leq 4\left(|X_{t_i^j}|_2^2 + |Y^\theta_{t_i^j}|_2^2 + |Y^\theta_{t_i^j}|_2^2 + |Y^\theta_{t_i^j-}|_2^2\right) \\ &\leq 4\left(|X_{t_i^j}|_2^2 + 3\kappa(n^j)^2\right). \end{aligned}$$

Hence, we obtain that

$$h(\theta, \xi_j) = \frac{1}{n^j}\sum_{i=1}^{n^j} F(\theta, X_{t_i^j}, Y_{t_i^j}, Y_{t_i^j-})^2 \leq 12\kappa\,(n^j)^2 + \frac{4}{n^j}\sum_{i=1}^{n^j}\left|X_{t_i^j}\right|_2^2,$$

implying that

$$\mathbb{E}_{\mathbb{P}\times\tilde{\mathbb{P}}}\left[\sup_{\theta\in\tilde{\Theta}_M} h(\theta, \xi_j)\right] \leq 12\kappa\,\mathbb{E}_{\tilde{\mathbb{P}}}\left[n^2\right] + 4\,\mathbb{E}_{\mathbb{P}\times\tilde{\mathbb{P}}}\left[\frac{1}{n}\sum_{i=1}^{n}|X_{t_i}|_2^2\right] < \infty, \tag{44}$$

using $(\mathcal{P}_3)$ of Lemma E.15 and the stronger assumption that n is square integrable. By $(\mathcal{P}_2)$ of Lemma E.15, the function $\theta \mapsto h(\theta)$ is continuous. Therefore, we can apply Lemma E.14, yielding that almost-surely for $N \to \infty$ the function

$$\theta \mapsto \frac{1}{N}\sum_{j=1}^{N} h(\theta, \xi_j) = \hat{\Phi}_N(\theta) \tag{45}$$

converges uniformly on $\tilde{\Theta}_M$ to

$$\theta \mapsto \mathbb{E}_{\mathbb{P}\times\tilde{\mathbb{P}}}[h(\theta, \xi_1)] = \Phi(\theta). \tag{46}$$

We deduce from Lemma E.13 that $d(\theta^{\min}_{M,N}, \Theta^{\min}_M) \to 0$ a.s. when $N \to \infty$. Then there exists a sequence $(\hat{\theta}^{\min}_{M,N})_{N\in\mathbb{N}}$ in $\Theta^{\min}_M$ such that $|\theta^{\min}_{M,N} - \hat{\theta}^{\min}_{M,N}|_2 \to 0$ a.s. for $N \to \infty$. The uniform continuity of the random functions $\theta \mapsto Y^\theta_t$ on $\tilde{\Theta}_M$ implies that $|Y^{\theta^{\min}_{M,N}}_t - Y^{\hat{\theta}^{\min}_{M,N}}_t|_2 \to 0$ a.s. when $N \to \infty$ for all $t \in [0, T]$. By continuity of F this yields $|h(\theta^{\min}_{M,N}, \xi_1) - h(\hat{\theta}^{\min}_{M,N}, \xi_1)|_2 \to 0$ a.s. as $N \to \infty$. With (44) we can apply dominated convergence which yields

$$\lim_{N\to\infty} \mathbb{E}_{\mathbb{P}\times\tilde{\mathbb{P}}}\left[|h(\theta^{\min}_{M,N}, \xi_1) - h(\hat{\theta}^{\min}_{M,N}, \xi_1)|_2\right] = 0.$$

Since for every integrable random variable Z we have $0 \leq |\mathbb{E}[Z]|_2 \leq \mathbb{E}[|Z|_2]$ and since $\hat{\theta}^{\min}_{M,N} \in \Theta^{\min}_M$ we can deduce

$$\lim_{N\to\infty} \Phi(\theta^{\min}_{M,N}) = \lim_{N\to\infty} \mathbb{E}_{\mathbb{P}\times\tilde{\mathbb{P}}}\left[h(\theta^{\min}_{M,N}, \xi_1)\right] = \lim_{N\to\infty} \mathbb{E}_{\mathbb{P}\times\tilde{\mathbb{P}}}\left[h(\hat{\theta}^{\min}_{M,N}, \xi_1)\right] = \Phi(\theta^{\min}_M). \tag{47}$$

Now by triangle inequality,

$$|\hat{\Phi}_N(\theta^{\min}_{M,N}) - \Phi(\theta^{\min}_M)| \leq |\hat{\Phi}_N(\theta^{\min}_{M,N}) - \Phi(\theta^{\min}_{M,N})| + |\Phi(\theta^{\min}_{M,N}) - \Phi(\theta^{\min}_M)|. \tag{48}$$

(45), (46) and (47) imply that both terms on the right hand side converge to 0 when $N \to \infty$, which finishes the proof of the first part of the Theorem.

We define $N_0 := 0$ and for every $M \in \mathbb{N}$

$$N_M := \min\left\{N \in \mathbb{N} \mid N > N_{M-1}, |\Phi(\theta^{\min}_{M,N}) - \Phi(\theta^{\min}_M)| \leq \tfrac{1}{M} + |\Phi(\theta^{\min}_M) - \Psi(\hat{X})|\right\},$$

which is possibly due to (47). Then Theorem E.2 implies that

$$|\Phi(\theta^{\min}_{M,N_M}) - \Psi(\hat{X})| \leq \tfrac{1}{M} + 2|\Phi(\theta^{\min}_M) - \Psi(\hat{X})| \xrightarrow{M\to\infty} 0.$$

Therefore, we can apply the same arguments as in the proof of Theorem E.2 (starting from (40)) to show that

$$\mathbb{E}_{\mathbb{P}\times\lambda_k}\left[\left|\hat{X} - Y^{\theta^{\min}_{M,N_M}}\right|_2\right] \leq c\,\tilde{c}\,\left(\Phi(\theta^{\min}_{M,N_M}) - \Psi(\hat{X})\right)^{1/2} \xrightarrow{M\to\infty} 0,$$

for every $1 \leq k \leq K$. □

Corollary E.16. *In the setting of Theorem E.12, we also have that* $(\mathbb{P} \times \tilde{\mathbb{P}})$*-a.s.*

$$\Phi(\theta^{\min}_{M,N_M}) \xrightarrow{N\to\infty} \Psi(\hat{X}) \quad \textit{and} \quad \hat{\Phi}_{\tilde{N}_M}(\theta^{\min}_{M,\tilde{N}_M}) \xrightarrow{N\to\infty} \Psi(\hat{X}),$$

where $(\tilde{N}_M)_{M\in\mathbb{N}}$ *is another increasing sequence in* $\mathbb{N}$.

Proof. The first convergence result was already shown in the proof of Theorem E.12 and the second one can be shown similarly, when defining $\tilde{N}_M$ by $\tilde{N}_0 := 0$ and for every $M \in \mathbb{N}$

$$\tilde{N}_M := \min\left\{N \in \mathbb{N} \mid N > \tilde{N}_{M-1}, |\hat{\Phi}_N(\theta^{\min}_{M,N}) - \Phi(\theta^{\min}_M)| \leq \tfrac{1}{M} + |\Phi(\theta^{\min}_M) - \Psi(\hat{X})|\right\},$$

which is possibly due to (48). □

E.3 Discussion about optimal weights

In Theorem E.2 and E.12, the focus lies on the convergence analysis under the assumption that optimal weights are found. Below we discuss, why this assumption is not restrictive in theory.

Global versus local optima. The assumption that the optimal weights are found, is typical for a convergence analysis of a neural network based algorithm, since the objective function is highly complex and non-convex with respect to the weights. In particular, it is well known that the standard choice of (stochastic) gradient descent optimization methods do in general only find local and not global minima. Since the difference between any local minimum and the global minimum can not generally be bounded, it is unrealistic to hope for a theoretical proof of convergence with respect to such optimisation schemes. On the other hand, global optimization methods as for example simulated annealing provably convergence (in probability) to a global optimum (Locatelli, 2000; Lecchini-Visintini et al., 2008). Hence, combining those with our result, convergence in probability of our model output to the conditional expectation can be established, without the assumption that the optimal weights are found. However, these global optimization schemes come at the cost of much slower training compared to (stochastic) gradient descent methods when applied in practice. Moreover, several works have focused on showing that most local optima of neural networks are nearly global, see for example (Feizi et al., 2017) and the related work therein. Hence, using (stochastic) gradient descent optimization methods likely yield nearly globally optimal weights much more efficiently. In our case, this is also supported by our empirical convergence studies in Section 6.3.

F EXPERIMENTAL DETAILS

All implementations were done using PyTorch. The code is available.

F.1 IMPLEMENTATION DETAILS

Dataset. For each of the SDE models (Black-Scholes, Ornstein-Uhlenbeck, Heston) a dataset was generated by sampling $N = 20'000$ paths of the SDE using the Euler-scheme. We used an equidistant time grid of mesh 0.01 between time 0 and $T = 1$. Independently for each path, observation times were sampled from $\mathbb{P}_t$, by using each of the grid points with probability 0.1 as an observation time. In particular, $n \sim \text{Bin}(100, 0.1)$, $t_0 = 0$ and the observation times $\{t_i\}_{1 \leq i \leq n}$ were chosen uniformly on the time grid. Hence, 10% of the grid points were used on average. This way, n and t_i are defined as a discretized version of those given in Example A.2 where n is binomially distributed and t_i chosen uniformly on $[0, T]$. For each of these datasets, the samples were used in a $80\%/20\%$ split for training and testing. The SDEs of the dataset models and the chosen parameters are described below.

- **Black-Scholes:**
  - SDE: $dX_t = \mu X_t dt + \sigma X_t dW_t$, where W is a 1-dimensional Brownian motion
  - conditional expectation: $E(X_{t+s}|X_t) = X_t e^{\mu s}$
  - used parameters: $\mu = 2$, $\sigma = 0.3$, $X_0 = 1$
- **Ornstein-Uhlenbeck:**
  - SDE: $dX_t = -k(X_t - m)dt + \sigma dW_t$, where W is a 1-dimensional Brownian motion
  - conditional expectation: $E(X_{t+s}|X_t) = X_t e^{-ks} + m\left(1 - e^{-ks}\right)$
  - used parameters: $k = 2, m = 4, \sigma = 0.3, X_0 = 1$
- **Heston:**
  - SDE: for W and Z 1-dimensional Brownian motions

$$dX_t = \mu X_t dt + \sqrt{v_t} X_t dW_t$$
$$dv_t = -k(v_t - m)dt + \sigma \sqrt{v_t} dZ_t$$

  - conditional expectation[8]: $E(X_{t+s}|X_t) = X_t e^{\mu s}$
  - used parameters: $\mu = 2$, $\sigma = 0.3$, $X_0 = 1$ $k = 2$, $m = 4$, $v_0 = 4$, $\rho = \text{Corr}(W, Z) = 0.5$

Architecture. In our experiments we choose the dimension of the latent variable to be $d_H = 10$. For f_{θ_1}, $\tilde{g}_{\theta_3}$ and $\tilde{\rho}_{\theta_2}$ we use 2-hidden-layer feed-forward neural networks, with 50 nodes in each hidden layer and $\tanh$ activation functions. Then the neural networks g_{θ_3} and ρ_{θ_2} are defined as residual versions of $\tilde{g}_{\theta_3}$ and $\tilde{\rho}_{\theta_2}$, by adding a residual shortcut between the input and the output of the neural networks. Moreover, also to the input of g_{θ_3} a $\tanh$ was applied, for reasons of symmetry. Dropout was applied after each non-linearity with a rate of 0.1. As we applied $\tanh$ to the possibly unbounded inputs x and h in every neural network, there was no further need to normalize or scale the data. To solve the ODE of the neural ODE part, the simple Euler-method was used.

Training. The neural networks were trained using the Adam optimizer (Kingma & Ba, 2014) with a learning rate of 0.001 and weight decay 0.0005 for 200 epochs using a batch size of 200. A random initialization was used and no hyper-parameter optimization was needed.

Further training results. Further training results on test samples are shown in Figure 8, 9, 10.

F.2 EXPERIMENTS ON OTHER DATASETS

We test our framework on additional synthetic datasets.

[8] see (Rujivan & Zhu, 2012, Equation 2.9)

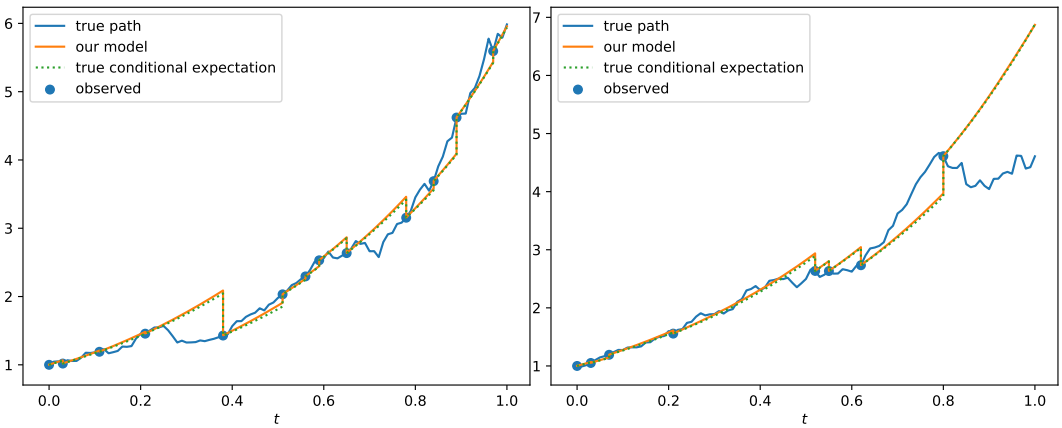

Figure 8: Black-Scholes

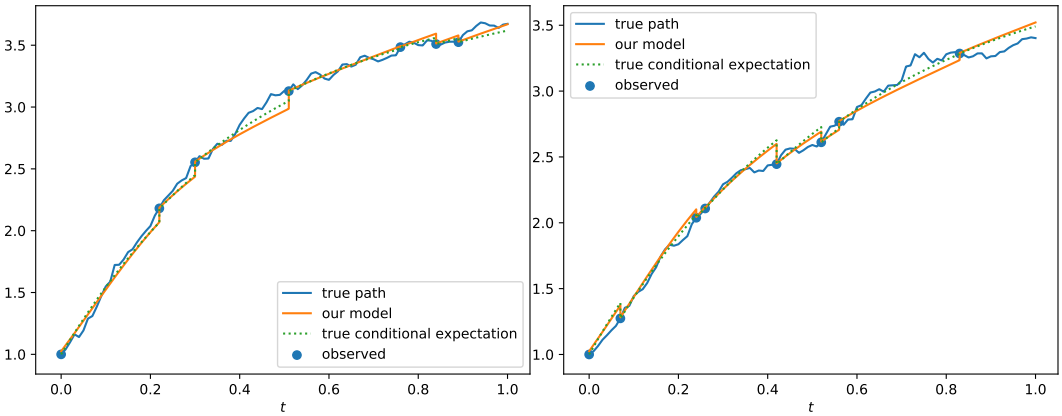

Figure 9: Ornstein-Uhlenbeck

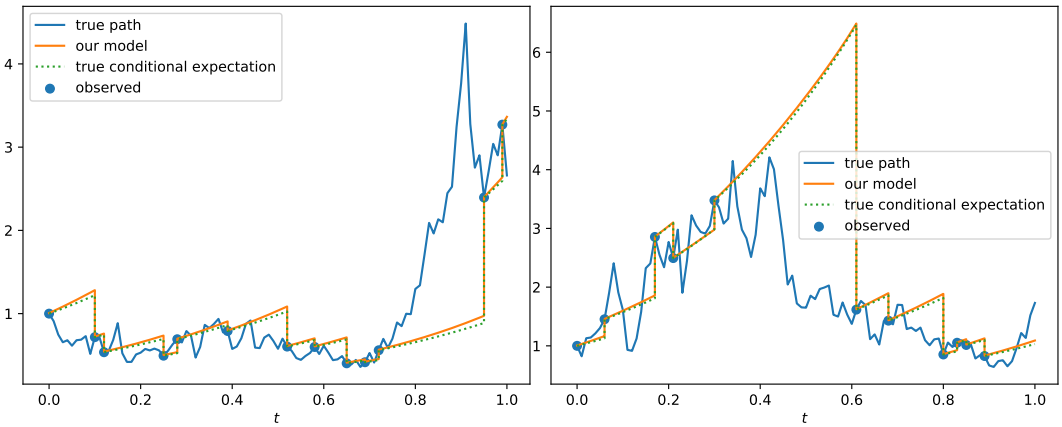

Figure 10: Heston

F.2.1 HESTON MODEL WITHOUT FELLER CONDITION

If the Feller condition

$$2\,k\,m \geq \sigma^2$$

is satisfied in the Heston model, it is known that the variance process v_t is always strictly bigger than 0 and that the Euler-scheme works well to sample from it. However, if the Feller condition is not satisfied, the variance process can touch 0, where the process is reflected deterministically. Then the Euler-scheme can not longer be used to sample from the model. Moreover, this situation is generally considered as more delicate. When close to 0 the distribution of v_t behaves differently than further away of 0 (Andersen, 2007, Section 3). As explained by Andersen (2007), there are differently well performing sampling schemes for a Heston model where the Feller condition is not satisfied. We use the simplest to implement, which is a slight extension of the Euler scheme, where values of v_t below 0 are replaced by 0 (Andersen, 2007, Section 2.3). Although there is empirical evidence, that the resulting sampling distribution of v_t close to 0 is not correctly replicating the true distribution (Jean-François et al., 2015, Figure 2,3), this method already produces sufficiently good sample paths.

Dataset. Heston model, sampled as in Section F.1 with the extension described above. Used parameters: $\mu = 2$, $\sigma = 3$, $X_0 = 1$ $k = 2$, $m = 1$, $v_0 = 0.5$, $\rho = \mathrm{Corr}(W, Z) = 0.5$. Hence the Feller condition and also the weaker condition $4\,k\,m \geq \sigma^2$ discussed in (Jean-François et al., 2015, Section 3.2), are both not satisfied. We produce two datasets, a 1-dimensional one similar to before, where only X is stored and a 2-dimensional,one where both X and v are stored, hence also v is a target for prediction. Note that v has the same conditional expectation as the Ornstein-Uhlenbeck SDE. In the 2-dimensional dataset, X and v are always observed at the same time.

Architecture & Training. Same as in Section F.1, but with batch size 100.

Results. The model learns to replicate the true conditional expectation process, which is analytic, hence not effected by the sampling scheme. In particular, we see that our model is very robust, since even in the delicate case where the Feller condition is not satisfied and a sampling scheme is used, that does not perfectly replicate the true distribution, our model still works well. Due to the very similar results, in Figure 11 we only show plots on test samples of the 2-dimensional dataset, where X and v are predicted.

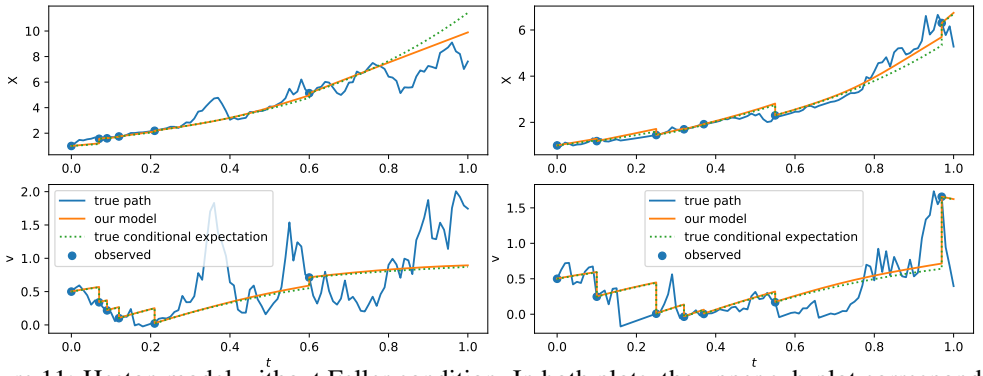

Figure 11: Heston model without Feller condition. In both plots, the upper sub-plot corresponds to the 1-dimensional path of X_t and the lower sub-plot corresponds to the 1-dimensional path of v_t.

F.2.2 DATASET WITH CHANGING REGIME

In this experiment we test, how well our model can deal with stochastic processes, that undergo an (abrupt) change of regime at a certain point in time. This constitutes a type of time dependence of the dynamics of the stochastic process. Many real world time series might exhibit such a change of regime. Some examples are:

- A stock market that suddenly changes from a bullish to a bearish market, for example due to a macro-economic event. An example for this would be the start of the Covid-19 crisis in the first quarter of 2020.

- Longitudinal patient health recordings might experience changes depending on seasonal or longer-term influences, as for example due to the seasonal flue or currently the Covid-19 pandemic.
- In many regions climate data has strong seasonal dependencies, that can lead to relatively abrupt changes as for example when the weather changes from dry to rain season.

Dataset. To be able to evaluate the performance of our model, we test a change of regime by combining two synthetic datasets. On the first half of the time interval $[0, 0.5]$ we use the Ornstein-Uhlenbeck and on the second half $[0.5, 1]$ the Black-Scholes model. The Black-Scholes process takes as starting point, the last point of the Ornstein-Uhlenbeck process. We use the same hyper-parameters for the dataset generation as in Section F.1, except that we set the parameter $m = 10$ in the Ornstein-Uhlenbeck model to make the two parts act on similar scales.

Architecture & Training. Same as in Section F.1, but with batch size 100. Moreover, we used 100 neurons in each hidden layer, to account for the more complicated setting, where also a time dependence has to be learnt.

Results. In the plots on test samples of the dataset shown in Figure 12 we see that our model correctly learns the change of regime.

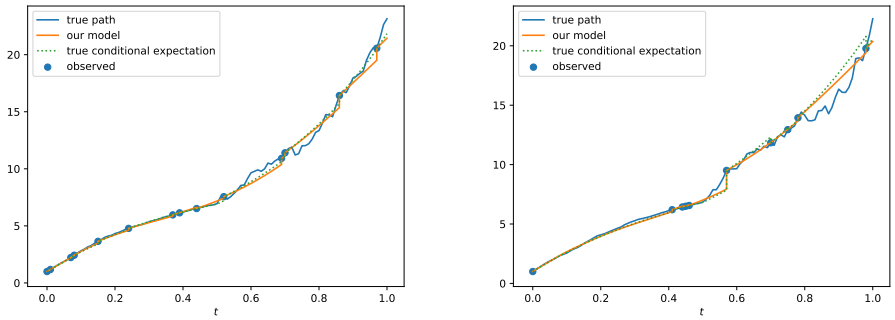

Figure 12: Our model evaluated on a stochastic dataset that follows an Ornstein-Uhlenbeck SDE on the time interval $[0, 0.5]$ and an Black-Scholes model on the time interval $(0.5, 1]$.

F.2.3 Dataset with explicit time dependence

Many real world datasets, have an explicit time dependence, i.e. the drift and diffusion of (10) explicitly depend on t. Examples are all datasets that have a certain periodicity, as for example weather data (seasonal and daily periodicity), intraday periodicity of stock prices (Andersen & Bollerslev, 1997) or prices of certain seasonal goods. We incorporate an explicit time dependence into the Black-Scholes dataset of Section F.1 to test how well our model can deal with such a situation.

Dataset. We use the Black-Scholes datasets of Section F.1, where we replace the constant μ by the time dependent constant $\frac{\alpha}{2}(\sin(\beta t) + 1)$, for $\alpha, \beta > 0$. The conditional expectation changes accordingly. For the data generation we use the same hyper-parameters as in Section F.1, except that we use instead of μ the parameter $\alpha = 2$ and $\beta \in \{2\pi, 4\pi\}$.

Architecture & Training. Same as in Section F.1, but with batch size 100. Moreover, we used 400 neurons in each hidden layer, to account for the more complicated setting, where an explicit time dependence has to be learnt.

Results. We show plots on test samples of the datasets in Figure 5. We see that the model learns to adapt to the time-dependent coefficients.

F.3 Details on convergence study

Evaluation metric. For the sampling time grid with equidistant step size $\Delta_t := \frac{T}{\nu}$, $\nu \in \mathbb{N}$, on $[0, T]$ and the true and predicted conditional expectation for path $j \in \mathbb{N}$, $\hat{X}^j$ and Y^j respectively, we define

the evaluation metric as

$$\text{eval}(\hat{X}, Y) := \frac{1}{N_2} \sum_{j=1}^{N_2} \frac{1}{\nu+1} \sum_{i=0}^{\nu} \left(\hat{X}^j_{i\Delta_t} - Y^j_{i\Delta_t} \right)^2, \tag{49}$$

where N_2 is the number of test samples, and j accordingly iterates over the paths in the test set.

Increasingly big training sets. We use the following procedure to create increasingly big training sets, while keeping the *exactly same* test set for evaluation. Out of the initial $20'000$ paths, we take $N_2 := 4'000$ paths, which are fixed as the testing set. Out of the remaining $16'000$ paths, we randomly choose N_1 training paths for $N_1 \in \{200, 400, 800, 1'600, 3'200, 6'400, 12'800\}$.

Increasing neural network sizes. The increasingly big neural networks are defined as follows. For all involved networks, we use the feed-forward 2-layer architecture with $\tanh$ activations (cf. Appedix F.1), where each hidden layer has the same size M for $M \in \{10, 20, 40, 80, 160, 320\}$.

Results on Black-Scholes dataset. In accordance with the theoretical results in Theorem E.2 and E.12, we see that the evaluation metric decreases when N_1 and M increase (Figure 13). It is important to notice, that already a quite small number of samples can lead to a good approximation of the conditional expectation, if the network is big enough. In particular, the Monte Carlo approximation of the theoretical loss function is good already with a few samples. On the other hand, even with a large number of samples, the evaluation metric does not become so small, if the network size is not big enough. From a practitioners point of view, this is good news, since increasing the network size is often much easier than collecting more training data.

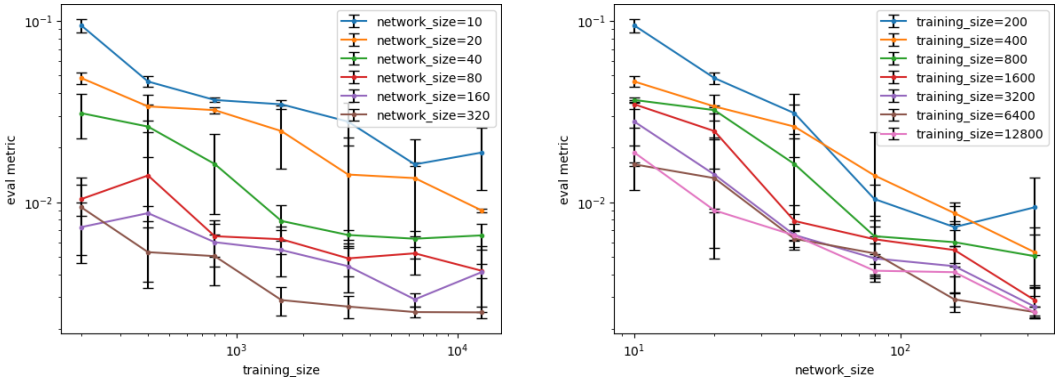

Figure 13: Black-Scholes dataset. Mean $\pm$ standard deviation (black bars) of the evaluation metric for varying N_1 and M.

Results on Ornstein-Uhlenbeck and Heston dataset. We get very similar results on the Ornstein Uhlenbeck (Figure 14) and Heston dataset (Figure 15). Similar as for Black Scholes, also for Ornstein-Uhlenbeck the training size N_1 is not as important as the network size M. For all network sizes, increasing the training size further than 1600 hardly changes the performance, while increasing M is crucial to get better performance. In contrast to this, for the Heston dataset we see that a large number of training samples is more important to get a smaller convergence metric. This reflects the fact, that the Heston dataset is more complex and more difficult to learn.

F.4 Details on comparison to GRU-ODE-Bayes

GRU-ODE-Bayes (Brouwer et al., 2019). To the best of our knowledge, this is the neural network based method with the most similar task to ours. In particular, this continuous time model is trained to learn the unknown temporal parameters of a normal distribution, best describing the conditional distribution of X given the previous observations. This distribution is given by the Fokker-Planck equation. Brouwer et al. (2019) outlined, that their model can exactly represent the Fokker-Planck dynamics of the Ornstein-Uhlenbeck process, since the corresponding distribution is Gaussian.

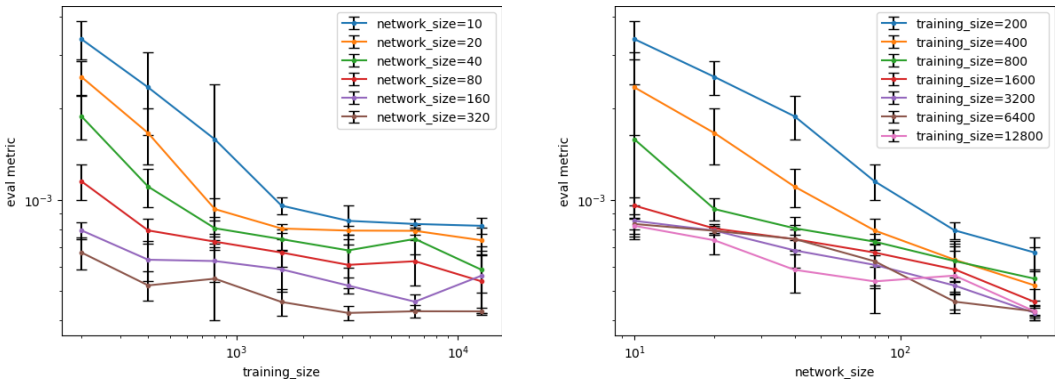

Figure 14: Ornstein-Uhlenbeck dataset. Mean $\pm$ standard deviation (black bars) of the evaluation metric for varying N_1 and M.

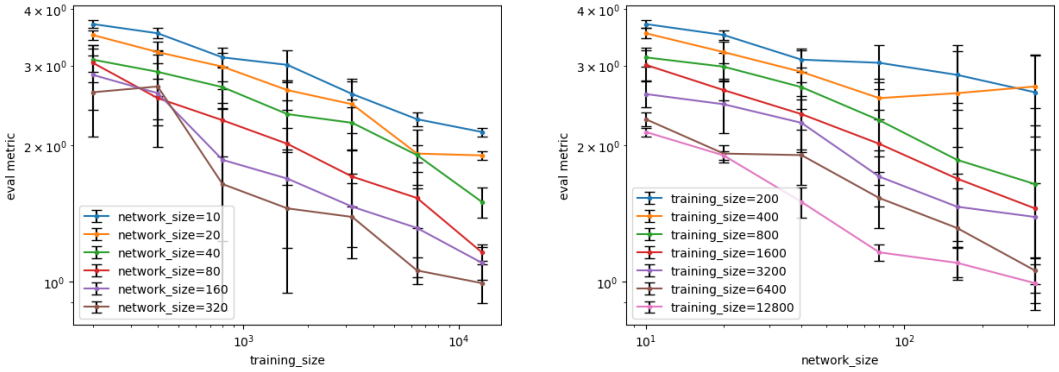

Figure 15: Heston dataset. Mean $\pm$ standard deviation (black bars) of the evaluation metric for varying N_1 and M.

Implementation of GRU-ODE-Bayes. We use the code of the official implementation of (Brouwer et al., 2019)[9] and slightly adjust it for our purpose. In particular, we do not use incomplete observations, hence the input mask used for this task has always only 1-entries. Furthermore, we slightly changed the scheme how the time steps are taken, to be the same as in our implementation, so that comparisons can be made. Besides these minor changes, the original model is used and trained on all 3 datasets (Black-Scholes, Ornstein-Uhlenbeck and Heston). We tried out all combinations of the following parameters and always chose the best performing one for comparison to our model: $\text{impute} \in \{\text{True}, \text{False}\}$, $\text{logvar} \in \{\text{True}, \text{False}\}$, $\text{mixing} \in \{0.0001, 0.5\}$ and $\text{hiddensize} \in \{50, 100\}$, whereby phidden and prephidden were chosen to be equal to hiddensize. The first parameter choices were the ones used in the official implementation. The model was always trained using the Euler-method for solving ODEs and with $\text{dropout} = 0.1$, to be comparable to our implementation. Furthermore, we always used the full GRU-ODE-Bayes implementation, since it should be the more powerful one. For the comparison, we only use the estimated mean of the normal distribution (the estimated variance is not used), which is precisely the estimated conditional expectation of the model.

Implementation of NJ-ODE. Same as described in Section F.1. For each dataset only one model was trained, since we already saw the convergence properties before and wanted to have a qualitative comparison to GRU-ODE-Bayes. In particular, we did not try to optimize our hyper-parameters for best performance (e.g. by choosing different number of layers or neurons or different activation functions) and used about $10K$ trainable parameters compared to the best performing GRU-ODE-Bayes models of our study which used $112K$ trainable parameters.

[9] https://github.com/edebrouwer/gru_ode_bayes

Datasets. Same as described in Section F.1. The train and test sets were fixed to be the same for all trained models.

Training. All models were trained using the Adam optimizer (Kingma & Ba, 2014) with a learning rate of 0.001 and weight decay 0.0005 for 100 epochs using a batch size of 20. A random initialization was used.

F.4.1 FURTHER RESULTS AND DISCUSSION OF THE COMPARISON

Evolution of losses and evaluation metric during training. In Figure 16 and 17 we see, that already after a few epochs the NJ-ODE model finds close to optimal weights for the given network size on the Black-Scholes and Orstein-Uhlenbeck dataset and oscillates around this optimum. The Heston dataset is considerably more difficult and the model slowly converges to close-to-optimal weights for the given network size. In comparison to this, it takes the GRU-ODE-Bayes model longer to converge to its close-to-optimal weights on the Black-Scholes and Orstein-Uhlenbeck dataset. Moreover, the model does not converge to close-to-optimal weights on the Heston dataset, but rather oscillates between bad weights. Due to some very large outliers, this is not directly visible in the plot, but can be deduced from Table 6.4.

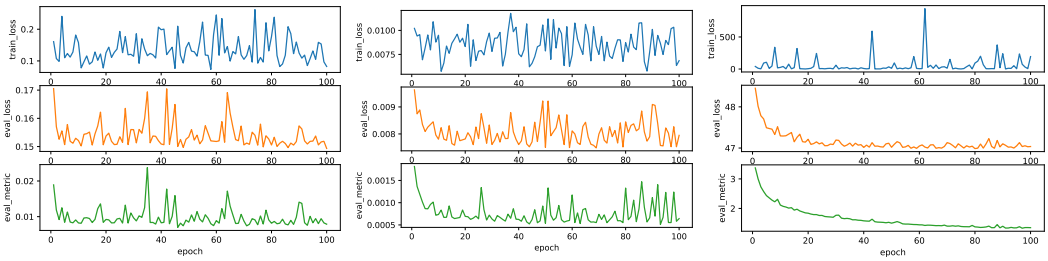

Figure 16: NJ-ODE on Black-Scholes, Ornstein-Uhlenbeck and Heston (from left to right). Blue (1st row): training loss, orange (2nd row): evaluation loss, green (3rd row): evaluation metric.

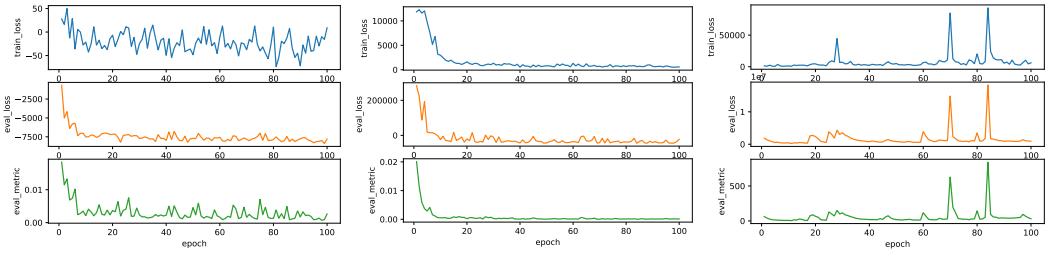

Figure 17: GRU-ODE-Bayes' best performing models on Black-Scholes, Ornstein-Uhlenbeck and Heston (from left to right). Blue (1st row): training loss, orange (2nd row): evaluation loss, green (3rd row): evaluation metric.

Comparison of predicted paths. For each dataset we show 5 paths that were predicted with NJ-ODE and with GRU-ODE-Bayes, first at the optimal epoch, i.e. where the test loss was minimal during training (Figures 18, 19, 20), and then at the last epoch (Figures 21, 22, 23). For the sake of comparison, in each row the performance on the same test sample is shown. The results are very similar for NJ-ODE and GRU-ODE-Bayes on the Black-Scholes and Ornstein-Uhlenbeck dataset, with sometimes the one and sometimes the other having a slightly better prediction. On the Heston dataset, the results of NJ-ODE are good predictions, being correct whenever a new observation is made and not too far away even after longer periods without observations. On the other hand, GRU-ODE-Bayes is not even correct at times of new observations and learns an incorrect behaviour in between observations (e.g. making kinks where there should not be any). For the last epoch, we see that this malfunction is amplified.

F.4.2 FURTHER EXPERIMENTS

Since the results of GRU-ODE-Bayes were unexpectedly bad on the Heston dataset, we performed additional tests. In particular, we retrained the best combinations of GRU-ODE-Bayes with the larger batch size 100. For smaller versions of the network (S), i.e. with $hiddensize = prephidden = phidden = 50$ this stabilized the training, such that the models converged. Still, even at the best epoch, the models suffered from the same difficulties as explained in Section F.4.1. Increasing the $hiddensize$ by factor 2 to 100 (L), made the training unstable again, and the models did not converge any more. This gives more empirical evidence, that GRU-ODE-Bayes can not be reliably trained on more complex datasets, where the target conditional distributions differs to much from a normal distribution. In contrast to this, retraining NJ-ODE with batch size 100, once for the smaller version described in Section F (S), once for a larger version with 100 instead of 50 neurons in all hidden layers (M) and once with 200 neurons (L), yielded the expected results of better performance with larger networks. In particular, there is no instability for larger networks. In Table F.4.1 we show results of our model and of the best GRU-ODE-model for the given size.

Table 4: The minimal, last and average value of the evaluation metric (smaller is better) on the Heston dataset throughout the 100 epochs of training, together with the number of trainable parameters.

	min	last	average	params
GRU (M)	2.38	4.63	8.25	$28'802$
GRU (L)	5.58	17.39	1877.26	$112'602$
ours (S)	1.71	1.71	2.05	$10'071$
ours (M)	1.21	1.23	1.60	$35'121$
ours (L)	1.07	1.08	1.36	$130'221$

F.5 REAL WORLD DATASETS WITH INCOMPLETE OBSERVATIONS

F.5.1 SELF-IMPUTATION FOR INCOMPLETE OBSERVATIONS

In the theoretical description of our model, we always assumed that at each observation time all coordinates of X are observed. However, in many real world dataset, the observations are incomplete, i.e. only for some of the coordinates an observation is available. To deal with this, we propose the following self-imputation method. Whenever an observation $X_t \in \mathbb{R}^{d_X}$ is made the mask $m_t \in \{0,1\}^{d_X}$ tells whether the i-th coordinate of X_t is observed ($m_t^i = 1$) or not ($m_t^i = 0$). Then we use the prediction Y_{t-} of our model to generate the imputed observation vector

$$\tilde{X}_t := m_t \odot X_t + (\mathbf{1}_{d_X} - m_t) \odot Y_{t-},$$

where $\odot$ is the element-wise multiplication (Hadamar product) and $\mathbf{1}_{d_X} \in \mathbb{R}^{d_X}$ is the one-vector. Instead of X_t we use $(\tilde{X}_t, m_t)$ as an input for the jump part ρ_{θ_2}. The intuition behind this definition is the following. In the one dimensional case, if we do not make an observation, but input Y_{t-} as if it was an observation, we expect that this does not change the output Y_s for $s \geq t$. From this point of view, Y_{t-} does not provide any additional information for the model. Similarly, we expect that imputing Y_{t-} for unobserved coordinates does not provide any information about this coordinate to the model. However, since the model might learn to transfer the information about an observed coordinate to an unobserved one, we extend the input to also include the information which coordinates were observed. For the ODE part, we use $Y_{\tau(t)}$, which is the prediction after processing the input $\tilde{X}_t$, instead of $X_{\tau(t)}$. Here the intuition is that if the model learns how to best use the incomplete observation, i.e. if the jump is good, then this is the best approximation for $X_{\tau(t)}$. In accordance, the loss function is adjusted to only use the non-imputed coordinates, i.e. if m is the random process in $\{0,1\}^{d_X}$ describing which coordinates are observed we have

$$\Psi(Z) := \mathbb{E}_{\mathbb{P}\times\tilde{\mathbb{P}}}\left[\frac{1}{n}\sum_{i=1}^{n}\left(|m_{t_i} \odot (X_{t_i} - Z_{t_i})|_2 + |m_{t_i} \odot (Z_{t_i} - Z_{t_i-})|_2\right)^2\right].$$

F.5.2 CLIMATE FORECASTING DETAILS

Dataset. We use the publicly available United State Historical Climatology Network (USHCN) daily dataset (Menne et al., 2016) together with all pre-processing steps as they were provided by Brouwer

et al. (2019). In particular, there are 5 sporadically observed (i.e. incomplete observations) climate variables (daily temperatures, precipitation, and snow) measured at $1'114$ stations scattered over the United States during an observation window of 4 years (between 1996 and 2000) where each station has an average of 346 observations over those 4 years. For 5 folds, the data is split into train (70%), validation (20%) and test (10%) sets. The task is to predict the next 3 measurements after the first 3 years of observation. The mean squared error between the prediction and the correct values is computed on the validation and test set.

Baselines. We use the results reported in (Brouwer et al., 2019, Table 1) as baselines for our comparison and perform the exact same 5-fold cross validation using the same folds with the same train, validation and test sets. For completeness, we give all results of the table together with our results in Table 6.5. We only show the mean squared error (MSE), since our model does not provide the negative log-likelihood.

Implementation of NJ-ODE. We once use the architecture described in Section F.1 (S) and once use the exact same architecture, but with hidden size $d_H = 50$ and 400 instead of 50 nodes in each hidden layer (L). To deal with the incomplete observations, the self-imputation scheme described in Section F.5 is used. In particular, the data is self-imputed and passed together with the observation mask as input to the network $\tilde{\rho}_{\theta_2}$. Moreover, the network f_{θ_1} uses the NJ-ODE output at the last observation time instead of the last observation as input.

Training. Both versions of NJ-ODE were trained using the Adam optimizer (Kingma & Ba, 2014) with a learning rate of 0.001 and weight decay 0.0005 for 100 epochs using a batch size of 100. A random initialization was used. The performance on the validation set was used for early stopping after the first 100 epochs, i.e. early stopping was possible at any epoch between $\{101, \dots, 200\}$.

Results. The results of our model and all models reported in (Brouwer et al., 2019, Table 1) are shown in Table 6.5.

F.5.3 PHYSIONET PREDICTION DETAILS

Dataset. We use the publicly available PhysioNet Challenge 2012 dataset (Goldberger et al., 2000) together with all pre-processing steps as they were described and provided by Rubanova et al. (2019). In particular, there are 41 features of 8000 patients that are observed irregularly over a 48 hour time period. The observation are put on a time grid with step size 0.016 hours leading to 3000 grid points. While in the paper Rubanova et al. (2019) say that they use 2880 grid points (i.e. minute wise) in their implementation they used 3000. Moreover, in contrast to what was written in the paper, the 4 constant features were not excluded in their implementation, hence we also keep them. Furthermore, we also rescale the time-grid to $[0, 1]$ and normalize each feature as Rubanova et al. (2019) did it for training the model. The dataset is split with the same fixed seed into 80% training and 20% test set. In particular, no cross validation but only multiple runs with new random initializations are performed to be exactly comparable to the results reported by Rubanova et al. (2019). On the test set, the observation paths are split in half. The first half (first 1500 time steps) is used as input for the model, from which the second half (second 1500 time steps) should be forecast. The masked mean squared error (MSE) with a certain balancing procedure between the predictions and the true values is reported. For comparability we use the exact same implementation of the MSE as Rubanova et al. (2019).

Baselines. We compare the performance of our model to latent ODE on the extrapolation task (as described above) on physionet. As baseline for our comparison we use the results reported in (Rubanova et al., 2019, Table 5). For completeness, we show all extrapolation results of the table together with our results in Table 6.5. We shortly outline the different approach of latent ODE compared to our model for the given extrapolation task. Latent ODE also splits the training samples similar to the test samples in half, using the first half as input and the second half as target. It is trained as an encoder-decoder, encoding the observations in the first half and reconstructing (decoding) the second half. This falls in the standard supervised learning framework. In particular, this approach cannot straight forward be extended for online forecasting. Moreover, this approach might learn certain path dependencies. On the other hand, our model is trained as always, online forecasting after each observation until the next observation is made. Instead of splitting the training samples we use the entire path as input for our unsupervised training framework. Our model is based on the assumption that paths are Markov, therefore it cannot learn path dependencies, i.e. dependencies

on more than just the last observation. However, by training the model also on the second half of the training samples, it learns the underlying behaviour there, which should be helpful for the extrapolation task.

Implementation of NJ-ODE. We use the architecture described in Section F.1, but with hidden size $d_H = 41$. To deal with the incomplete observations, the self-imputation scheme described in Section F.5 is used. In particular, the data is self-imputed and passed together with the observation mask as input to the network $\tilde{\rho}_{\theta_2}$. Moreover, the network f_{θ_1} uses the NJ-ODE output at the last observation time instead of the last observation as input.

Training. The NJ-ODE was trained using the Adam optimizer (Kingma & Ba, 2014) with a learning rate of 0.001 and weight decay 0.0005 for 175 epochs using a batch size of 50. 5 runs with random initialization were performed over which the mean and standard deviations were calculated. In particular, these runs always used the same training and test set, specified by the same random seed as in thee implementation of Rubanova et al. (2019).

Results. The results of our model and all models reported in (Rubanova et al., 2019, Table 5, extrapolation) are shown in Table 6.5. We report the minimal MSE on the test set during the 175 epochs, since it was not differently specified in (Rubanova et al., 2019). However, if the MSE of the epoch is used where the training loss is minimal, the results are nearly the same with 1.986 ± 0.058 ($\times 10^{-3}$). Moreover, we trained a larger model for 120 epochs, where 200 nodes were used instead of 50 ($187'323$ parameters in total), leading to slightly better results of 1.934 ± 0.007 ($\times 10^{-3}$) (at minimal MSE) and 1.982 ± 0.027 ($\times 10^{-3}$) (at minimal training loss).

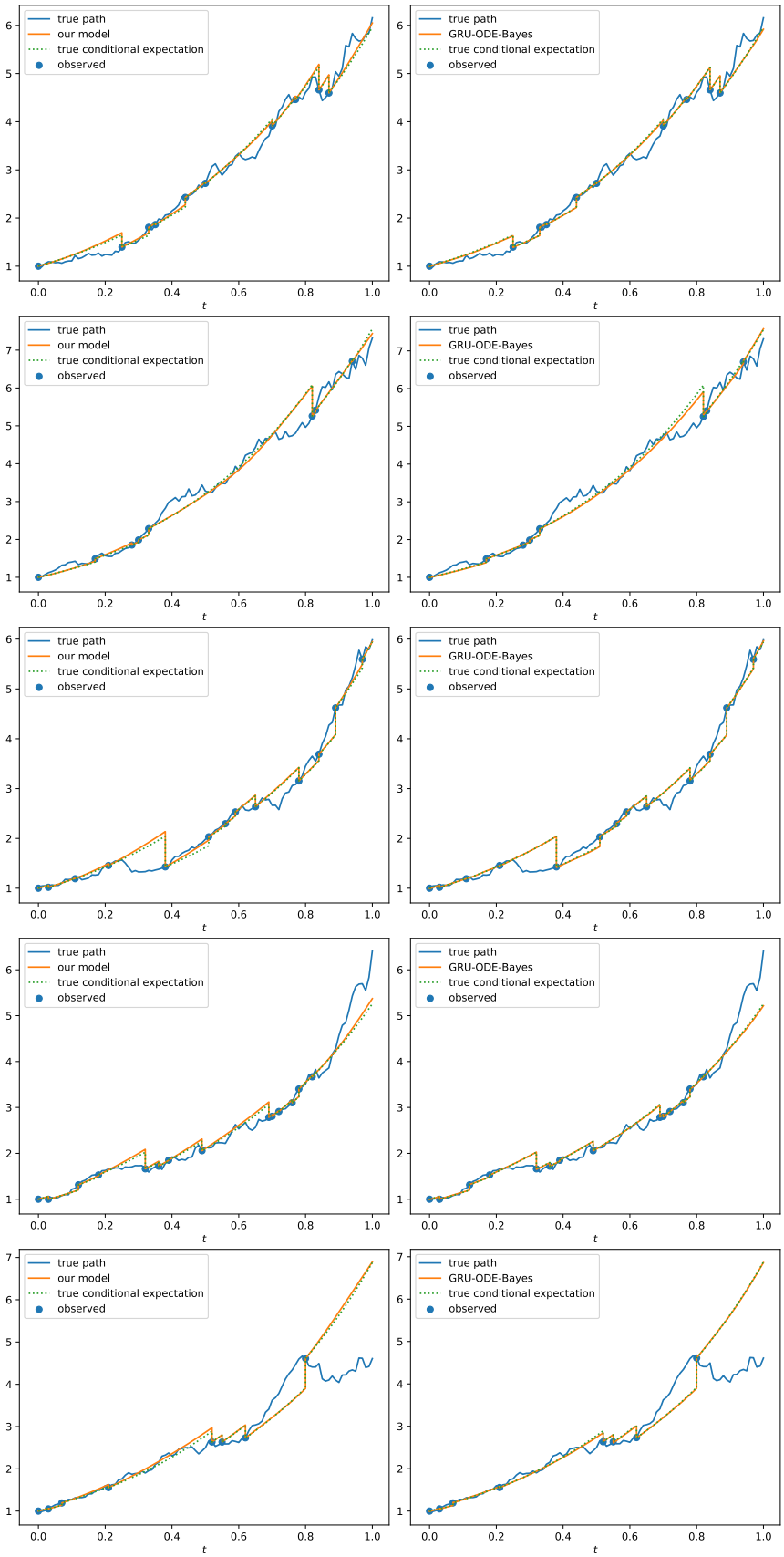

Figure 18: Comparison of predictions for Black-Scholes paths at best epoch.

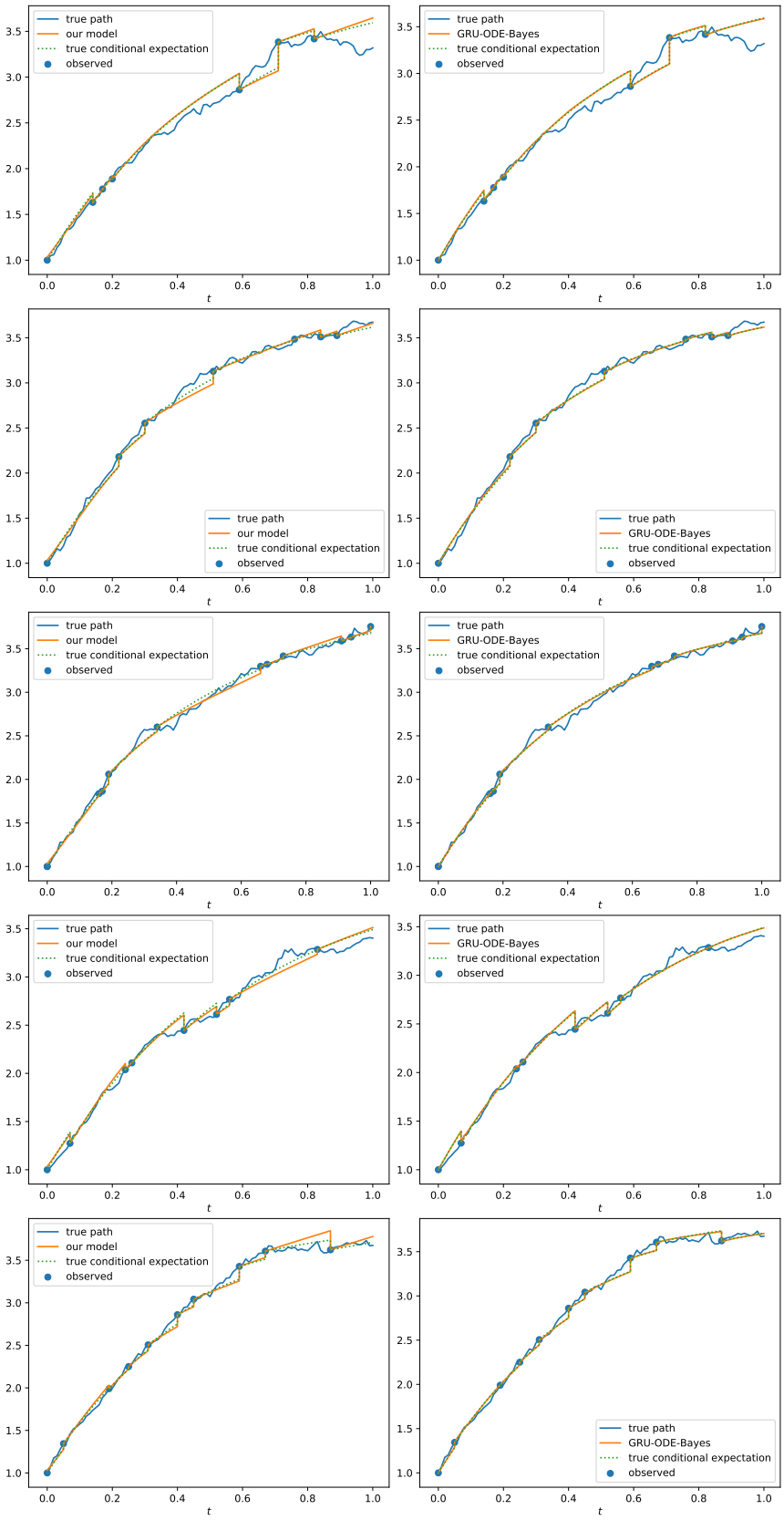

Figure 19: Comparison of predictions for Ornstein-Uhlenbeck paths at best epoch.

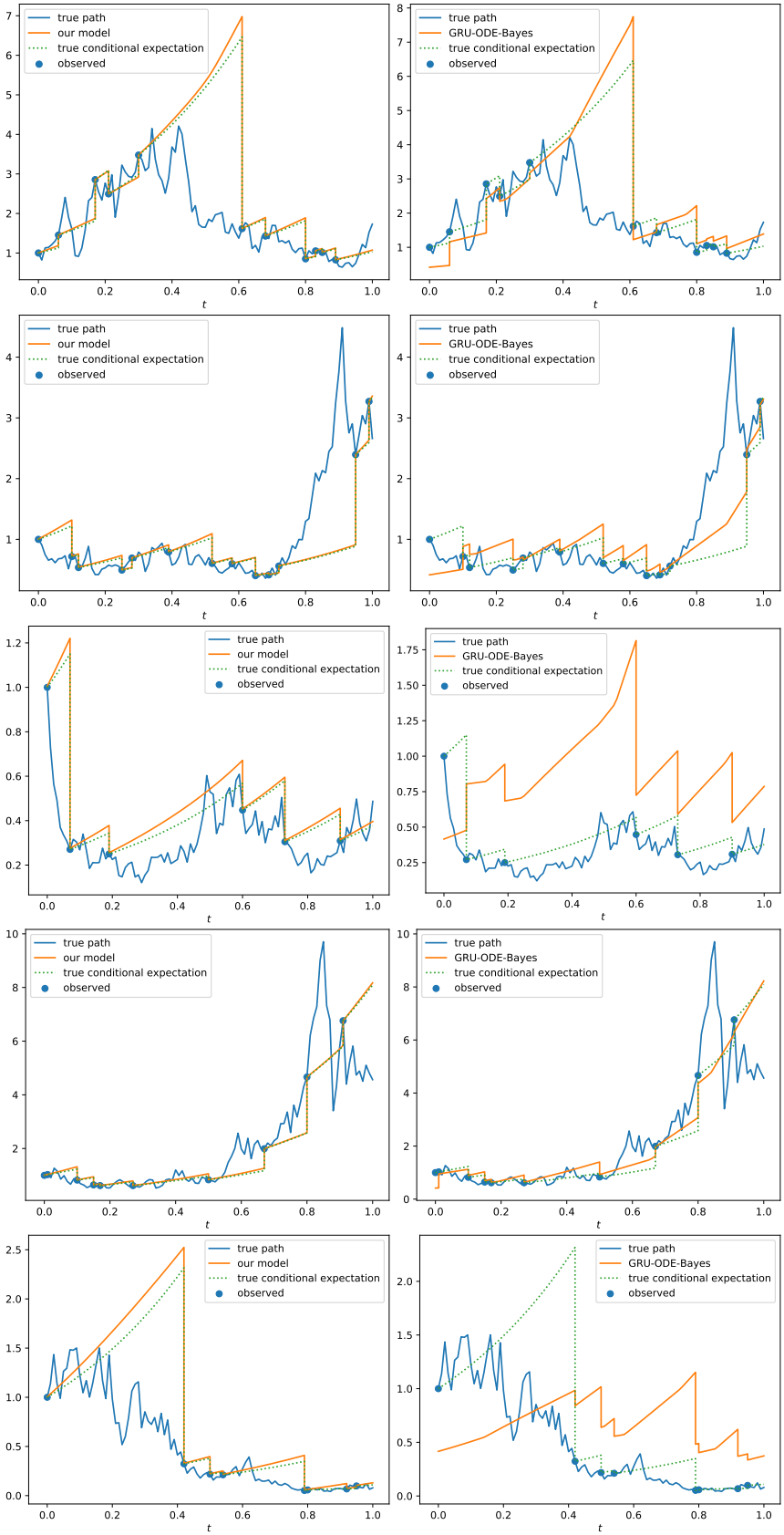

Figure 20: Comparison of predictions for Heston paths at best epoch.

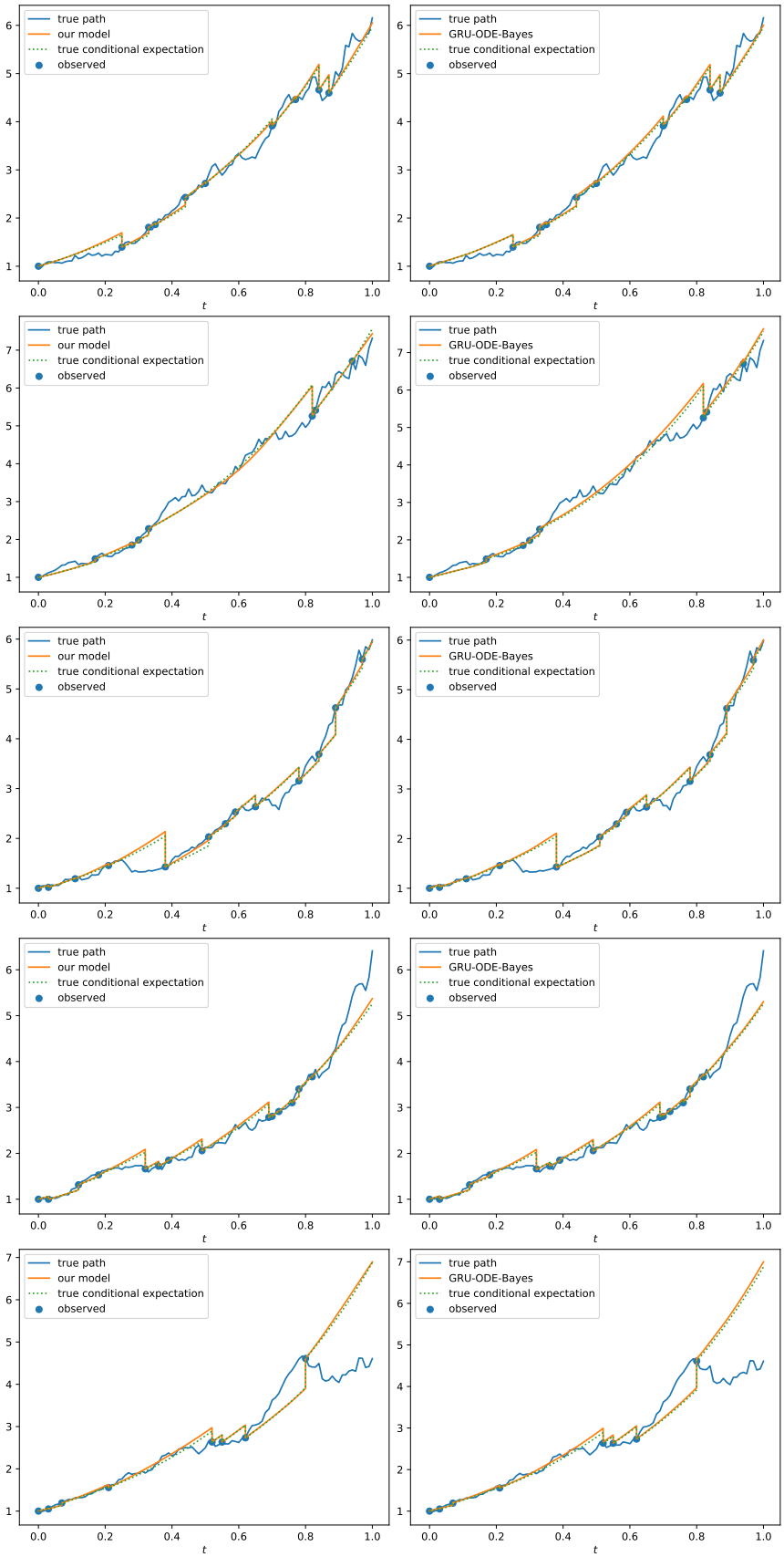

Figure 21: Comparison of predictions for Black-Scholes paths at last epoch.

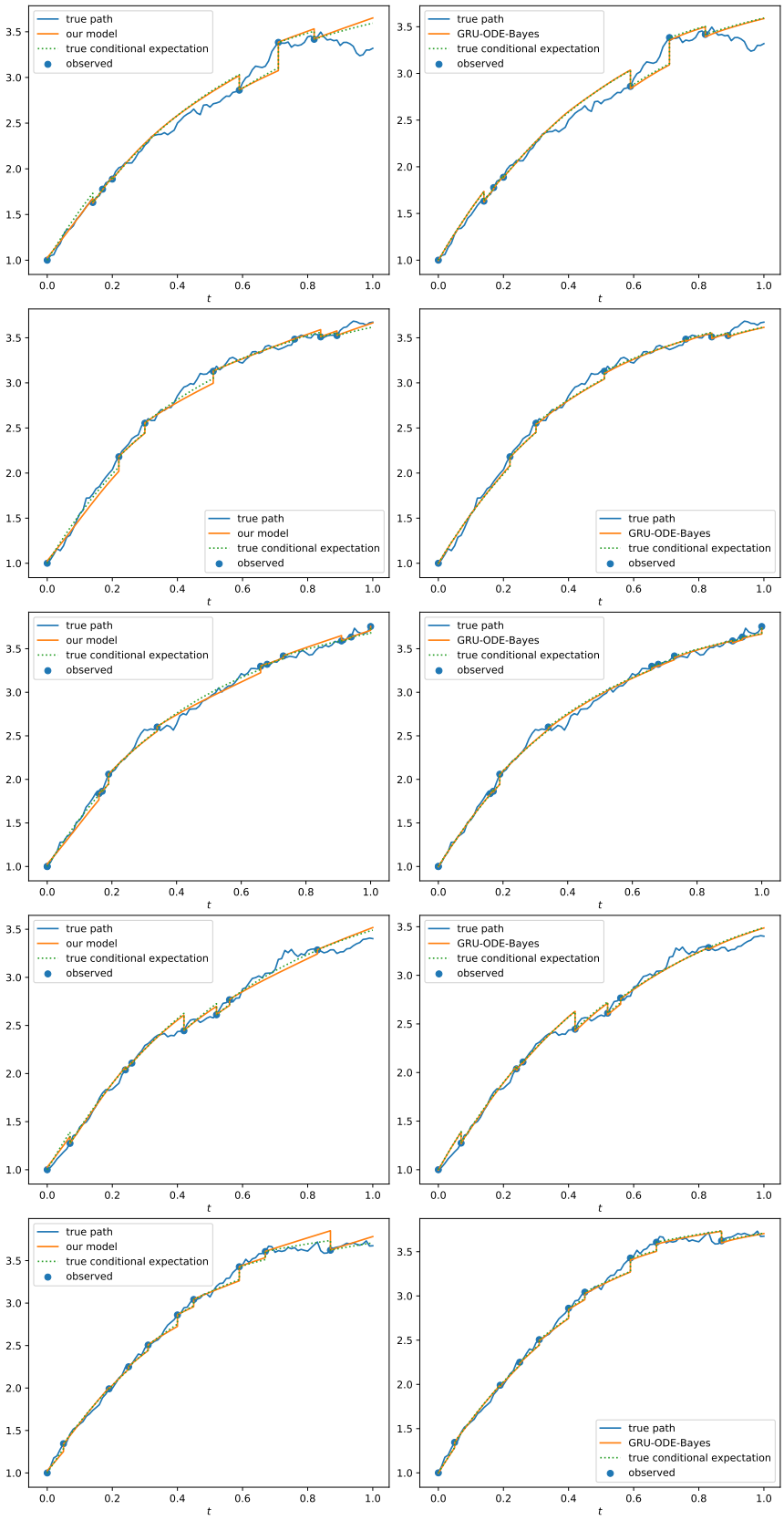

Figure 22: Comparison of predictions for Ornstein-Uhlenbeck paths at last epoch.

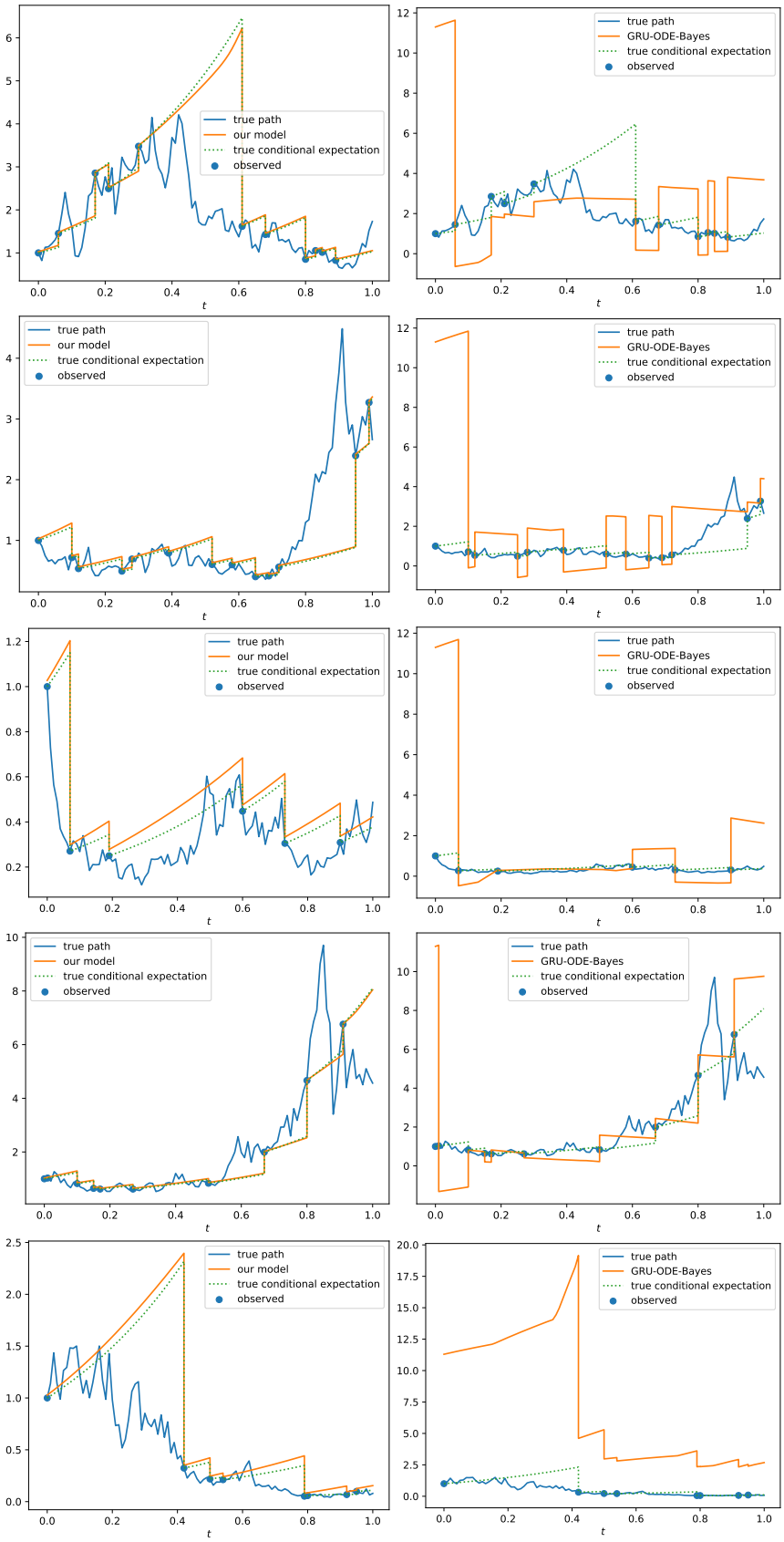

Figure 23: Comparison of predictions for Heston paths at last epoch.